Phosphorylation of the synaptonemal complex protein SYP-1 promotes meiotic chromosome segregation

Aya Sato-Carlton, Chihiro Nakamura-Tabuchi, Stephane Kazuki Chartrand, Tomoki Uchino, and Peter Mark Carlton

Graduate School of Biostudies, Kyoto University, Kyoto, Japan

Chromosomes that have undergone crossing over in meiotic prophase must maintain sister chromatid cohesion somewhere along their length between the first and second meiotic divisions. Although many eukaryotes use the centromere as a site to maintain cohesion, the holocentric organism *Caenorhabditis elegans* instead creates two chromosome domains of unequal length termed the short arm and long arm, which become the first and second site of cohesion loss at meiosis I and II. The mechanisms that confer distinct functions to the short and long arm domains remain poorly understood. Here, we show that phosphorylation of the synaptonemal complex protein SYP-1 is required to create these domains. Once crossover sites are designated, phosphorylated SYP-1 and PLK-2 become cooperatively confined to short arms and guide phosphorylated histone H3 and the chromosomal passenger complex to the site of meiosis I cohesion loss. Our results show that PLK-2 and phosphorylated SYP-1 ensure creation of the short arm subdomain, promoting disjunction of chromosomes in meiosis I.

Introduction

The partitioning of single haploid genomes from a replicated diploid genome in meiosis requires that the four linked chromatids of each homologous chromosome pair come apart from each other in two successive divisions. Throughout these two divisions, chromosomes are held together by sister chromatid cohesion. Cohesion must therefore be released in two discrete steps, so that chromosomes remain linked between the first and second division. Organisms with monocentric chromosomes first release cohesion from chromosome arms in meiosis I but protect cohesion at the centromere using the protein Shugoshin (Kitajima et al., 2004); cohesion at the centromere is only released in the second division. Many organisms, including *Caenorhabditis elegans*, have holocentric chromosomes (Dernburg, 2001; Melters et al., 2012), in which kinetochores are not restricted to a single locus but instead spread over the entire length of the chromosome. This arrangement presents a challenge to the two-step loss of chromosome cohesion, because predefined centromere and chromosome arm domains do not exist. In *C. elegans* meiosis, two-step cohesion loss is achieved by the facultative creation on each chromosome of two functionally distinct domains separated by the single crossover (CO; Martinez-Perez et al., 2008). Because the CO has a reliably off-center position (Barnes et al., 1995), these domains have different lengths and are termed the short arm, which loses cohesion in meiosis I, and the long arm, which retains cohesion until meiosis II (Lui and Colaiácovo, 2013). The mechanisms that determine the functional state of these domains in a length-dependent manner are not understood.

The synaptonemal complex (SC) is a macroassembly that plays critical roles in holding homologous chromosomes together (Zickler and Kleckner, 1999) and ensuring the correct distribution of COs (Hayashi et al., 2010) during meiotic prophase. The SC consists of axial elements, located on the long axis of each replicated chromosome, and the central element, which bridges the two axial elements (called lateral elements after synapsis). Previous studies have shown that several SC proteins disassemble asymmetrically from either short or long arms in diplotene and diakinesis, the prophase substages immediately before the first meiotic division. In wild-type animals, all the central element proteins (SYP-1, SYP-2, SYP-3, and SYP-4) disassemble from the long arms of bivalents in diplotene, remain on short arms through early diakinesis, and disappear completely by the −2 position (proceeding distally from the spermatheca, oocyte precursors in diakinesis are designated as stage −1, −2, −3, etc., oocytes; Nabeshima et al., 2005). Conversely, two of the four axial element proteins (HTP-1 and HTP-2) disassemble from short arms in diplotene and remain on long arms in diakinesis, whereas the remaining two (HTP-3 and HIM-3) persist on both short and long arms (Martinez-Perez et al., 2008). This asymmetric disassembly depends on the activity of Polo-like kinase 2 (PLK-2; Harper et al., 2011). PLK-2 first localizes to the meiotic pairing centers (PCs), DNA sequences that promote pairing in cis (Herman and Kari, 1989; McKim et al., 1993; Villeneuve, 1994; MacQueen et al., 2002; Phillips et al., 2005) in the leptotene/zygotene transition zone (TZ), and then relocalizes to the SC from early pachytene. PLK-2 itself becomes enriched on the short arm at late pachytene

Correspondence to Peter Mark Carlton: pcarlton@icems.kyoto-u.ac.jp

Supplemental material can be found at:
http://doi.org/10.1083/jcb.201707161

The Rockefeller University Press
J. Cell Biol.
https://doi.org/10.1083/jcb.201707161

(Pattabiraman et al., 2017). Although PLK-2 localization to the SC was shown to be dependent on SYP-1 (Harper et al., 2011), PLK-2 becomes confined to short arms earlier than SYP-1 does (Pattabiraman et al., 2017), leaving the mechanism of PLK-2 recruitment to the SC unexplained.

Previous studies have found SC-interacting proteins that also localize to chromosomes asymmetrically as SC proteins disassemble from either short or long arms. The protein LAB-1 forms a complex with lateral element proteins and protects cohesion on long arms at meiosis I (de Carvalho et al., 2008). LAB-1 localizes to the entire length of the SC from the TZ through pachytene and becomes confined to long arms in diplotene as SC components disassemble (de Carvalho et al., 2008). LAB-1 binds to protein phosphatase 1 (PP1), represented by orthologues *gsp-1* and *gsp-2* in *C. elegans*, and promotes the activity of GSP-1/2 (PP1) on the SC, antagonizing Aurora B kinase (de Carvalho et al., 2008; Tzur et al., 2012). Aurora B (*C. elegans* AIR-2) functions in a protein complex called the chromosomal passenger complex (CPC) together with INCENP (ICP-1), Borealin (CSC-1), and Survivin (BIR-1), which together play a crucial role in triggering cohesin cleavage during mitosis and meiosis (Carmena et al., 2012, 2014). The CPC also plays multiple roles in activating the spindle assembly checkpoint and destabilizing erroneous microtubule attachment to the kinetochore to ensure correct orientation of chromatids at cell division. Previous studies in *C. elegans* have shown that AIR-2 (Aurora B) localizes to short arms right before the meiosis I division and to the interface between sister chromatids before the meiosis II division (Kaitna et al., 2002; Rogers et al., 2002). AIR-2 phosphorylates the meiotic cohesin REC-8 to trigger cohesin removal and recruits spindle assembly checkpoint proteins (Kaitna et al., 2002; Rogers et al., 2002; Dumont et al., 2010). Because the CPC dictates the site of cohesion loss and chromosome separation, its localization is strictly regulated by multiple feedback loops (Carmena et al., 2012). In diverse eukaryotic cells, two histone marks, phosphorylated histone H3 threonine 3 (H3T3ph) and phosphorylated H2A threonine 120 (H2AT120ph) are bound by the CPC and CPC-interacting Shugoshin in mitosis (Kelly et al., 2010; Yamagishi et al., 2010). H3T3 is phosphorylated by Haspin kinase (Wang et al., 2010, 2011), and this is counterbalanced by the phosphatase activity of PP1 (Qian et al., 2011), whereas H2AT120 is phosphorylated by Bub1 kinase (Kawashima et al., 2010). Thus, chromatin carrying both phosphorylated histones functions as a docking site for the CPC. Although the mechanisms localizing the CPC to centromeres during mitosis in monocentric organisms have been well studied, how the CPC localizes to meiotic chromosomes in holocentric organisms is not well understood.

Posttranslational modification of the SC has been reported as a major aspect of its regulation (Fukuda et al., 2012; Jordan et al., 2012; Leung et al., 2015; Gao et al., 2016; Nadarajan et al., 2017). Here, we report a role for C-terminal phosphorylation of SYP-1 in establishing the functions of the short and long arms in stepwise cohesion loss in meiosis. Phosphorylated SYP-1 promotes PLK-2 localization to the SC, facilitating its departure from the PCs and progression of meiotic prophase. Upon CO designation, PLK-2 is required to enrich phosphorylated SYP-1 at the short arm, which in turn leads to restriction of PLK-2 itself to the short arm as well. Phosphorylation of SYP-1 precedes and is required for the asymmetric disassembly of SC components in late prophase and for the enrichment of CPC-recruiting histone marks on the short arms. Loss of SYP-1 phosphorylation therefore prevents the formation of asymmetric chromosome domains, leading ultimately to the mislocalization of the CPC and failures of the first meiotic division. This work establishes SYP-1 phosphorylation as a key upstream factor in the specification of chromosomal domains important for meiotic chromosome segregation.

Results

C-terminal phosphorylation of SYP-1 is required for meiotic competence

To gain insight into the possible roles of SC phosphorylation, we performed a phosphoproteomics analysis using mass spectrometry of phosphoprotein-enriched protein lysates from adult *C. elegans*, in which roughly half of the cells are oocyte precursor cells in meiotic prophase. We identified 12 phosphorylation sites at the C terminus of SYP-1 (Fig. 1 A and Table S1), 10 of which show conservation in other *Caenorhabditis* species (Fig. S1 A). To test whether phosphorylation of these residues is important for SYP-1 function in meiosis, we constructed a strain expressing a transgene with a nonphosphorylatable SYP-1 allele termed 12A, with all 12 potential phosphoresidues changed to alanine. In a background lacking the endogenous *syp-1* gene, the 12A allele displayed reduced viability (59.5% viable), and a high incidence of male progeny (Him) phenotype (6%; Fig. 1 B). The Him phenotype reflects meiotic X chromosome nondisjunction in XX hermaphrodite self-progeny, because worms with a single X (XO) develop as males. The *syp-1(me17)* null allele shows severely reduced viability (5% viable) and 38% males in the surviving self-progeny (MacQueen et al., 2002), indicating that *syp-1(12A)* is a partial loss-of-function allele. A wild-type SYP-1 transgene integrated at the same site as the 12A allele restored fertility to wild-type levels in the presence of *syp-1*(*me17*), showing that the defects in the 12A allele are specific to the introduced mutations. In oocytes undergoing the first meiotic division, we found anaphase chromosome bridges between separating chromatin masses (Fig. S1 B) in 12A and T452A mutants, but not in wild-type animals: 36% of anaphase I nuclei had chromosome bridges (n = 11 for both 12A and T452A), whereas no bridges were detected in the wild type (n = 15). This observation suggests that phosphorylation of the SYP-1 C terminus is required for proper chromosome segregation during meiosis.

Phosphorylation of SYP-1 Thr 452 is crucial to the function of SYP-1

To dissect the role of the SYP-1 phosphorylation sites, we made a series of transgenic worms expressing SYP-1 proteins with nonphosphorylatable mutations. First, we made *syp-1(4A)* mutants in which the first four phosphosites were converted to alanine, as well as *syp-1(8A)* mutants in which the last eight phosphosites were converted to alanine. The transgenic line expressing SYP-1(4A) showed no progeny inviability or Him phenotype, whereas the line expressing SYP-1(8A) showed inviability and male production comparable to the line expressing SYP-1(12A) (Fig. 1 B). The most strongly conserved region within these eight residues contains a putative S-[pS/pT]-P/X Polo-box domain (PBD)–binding motif, in which phosphorylation of the central Ser/Thr residue by a priming kinase (Elia et al., 2003) permits subsequent binding of PLK. Our phosphoproteomics analysis detected phosphorylated Thr^{452} in this putative

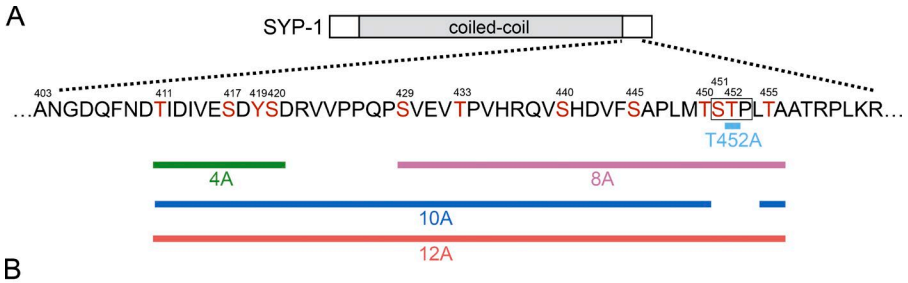

B

Genotype	Embryo Viability (%)	Male progeny (%) (Rate of X chr non-disjunction)	Total # eggs scored
N2 (wild type)	100.0	0.1	1276
syp-1 (wt); syp-1(me17)	100.0	0	1092
syp-1 (12A); syp-1(me17)	59.5	6.0	1716
syp-1 (10A); syp-1(me17)	99.9	1.7	1608
syp-1 (8A); syp-1(me17)	65.4	8.0	1553
syp-1 (4A); syp-1(me17)	100.0	0.1	879
syp-1 (T452A) ; syp-1(me17)	60.3	8.1	1028

Figure 1. **Phosphorylation of the C terminus of SYP-1 is required for correct chromosome segregation in meiosis. (A)** SYP-1 phosphorylation sites identified by mass spectrometry, and schematic diagram of a series of *syp-1* phospho mutants. Phosphorylation sites are depicted in red, and the conserved PBD-binding motif [STP] is boxed. For each mutant, the indicated Ser/Thr/Tyr residues are converted to Ala. **(B)** Percentage of viability and males among the self-progeny of worms with the indicated genotypes.

PBD-binding motif (Ser^{451}-Thr^{452}-Pro^{453}) at a higher level (55 peptide counts total) than the other phosphosites (ranging from 1 to 24 counts; Table S1). To test whether this putative PBD-binding motif is important for SYP-1 function, we generated *syp-1(T452A)* mutants in which Thr^{452} in the PBD-binding motif was converted to alanine, as well as a *syp-1(10A)* mutant in which the 10 phosphosites outside the PBD-binding motif were converted to alanine. The *syp-1(T452A)* mutants showed progeny inviability and male production similar to the 12A and 8A mutants. In contrast, *syp-1(10A)* mutants were fully viable and displayed only a weak Him phenotype (Fig. 1 B). This suggests that phosphorylation at the PBD-binding motif is crucial for SYP-1 function.

Phosphorylated SYP-1 concentrates on short arms of chromosomes after COs are designated

To investigate the timing and location of SYP-1 phosphorylation, we generated two different phospho-specific antibodies: one against a peptide from SYP-1's C terminus with phospho-threonine at Thr452 (1-phos antibody) and another against the same peptide phosphorylated at three residues (Thr450, Thr452, and Thr455 [3-phos antibody]). Immunofluorescence staining showed similar patterns with both antibodies but higher background with the 3-phos antibody; thereafter, the 1-phos antibody was consistently used to detect phosphorylated SYP-1. The specificity of the antibody to phospho-SYP-1 was confirmed by lack of staining in T452A mutants (Fig. S1 C). Using this antibody, we first observed phosphorylated SYP-1 signals in the TZ, coextant with pan-SYP-1 signals along the entire length of the SC (Fig. 2 A). As meiocytes progress into late pachytene, and the CO designation marker COSA-1 starts to appear, SYP-1-phos staining concentrates on short arms and decreases on long arms, whereas pan-SYP-1 signals are still detected along the entire SC (Fig. 2, B and C). In diplotene, SYP-1-phos signal intensity increases further on short arms, whereas pan-SYP-1 starts to disassemble from long arms, as previously shown (Martinez-Perez et al., 2008). The observation that SYP-1-phos signals begin to accumulate on short arms shortly after GFP::COSA-1 foci are detected suggested that COs trigger the confinement of SYP-1-phos to short arms. To test this hypothesis, we examined SYP-1-phos in gonads of *spo-11(me44)* mutants, which cannot initiate programmed double-strand breaks (DSBs) and therefore lack COs (Dernburg et al., 1998). In the absence of SPO-11, SYP-1-phos signals start to appear in the TZ but remain along the entire length of the SC through late pachytene and eventually disappear from the SC at the end of pachytene or diplotene (Fig. 2 D), providing evidence that DSBs are required for the asymmetric distribution of phosphorylated SYP-1.

The confinement of SYP-1-phos signals to short arms was reminiscent of the previously reported localization of PLK-2. PLK-2 first localizes to the PCs during zygotene by binding to HIM-8 and ZIM proteins, then relocates to the entire length of the SC in pachytene in a SYP-1–dependent manner, and later becomes confined to the short arms in a CO-dependent manner (Harper et al., 2011; Labella et al., 2011; Pattabiraman et al., 2017). We examined *syp-1(12A)* and *syp-1(T452A)* mutants and found that PLK-2 remained at PCs longer, eventually disappearing from the PCs in the region corresponding to late pachytene but failing to relocate to the SC (Fig. 3). This result strongly suggests that the phosphorylated PBD-binding motif of SYP-1 is required for PLK-2 localization to the SC in pachytene and subsequent stages. In contrast, in *syp-1(10A)* mutants, PLK-2 also remained at PCs longer but eventually did colocalize weakly to the SC in late pachytene (Fig. S1, D and E). Because PBD-binding motifs must be phosphorylated at the central threonine residue (Thr452 in SYP-1) to enable PLK2 recruitment, the conversion of the nearby Thr^{450} to alanine in the 10A mutant might lower priming phosphorylation at Thr^{452} or confer weaker affinity to PLK-2 itself.

To examine whether PLK-2 acts strictly downstream of SYP-1, we visualized SYP-1-phos in *plk-2* mutants. The *plk-2(ok1936)* null mutant shows delayed synapsis, but more than 60% of chromosomes do achieve homologous pairing and synapsis, and the number of COs made are sufficient for 33.8% progeny viability (8.4% male; Harper et al., 2011; Labella et al., 2011). The presence of meiocytes carrying COs in *plk-2 (ok1936)* mutants let us examine the confinement of phosphorylated SYP-1 to short arms in this mutant. We found that SYP-1 phosphorylation starting from the TZ is robustly detected in *plk-2(ok1936)* mutants but persists over the entire length of the SC in late pachytene, never becoming confined to short arms (Fig. 3 D). This observation suggests the existence of a feed-

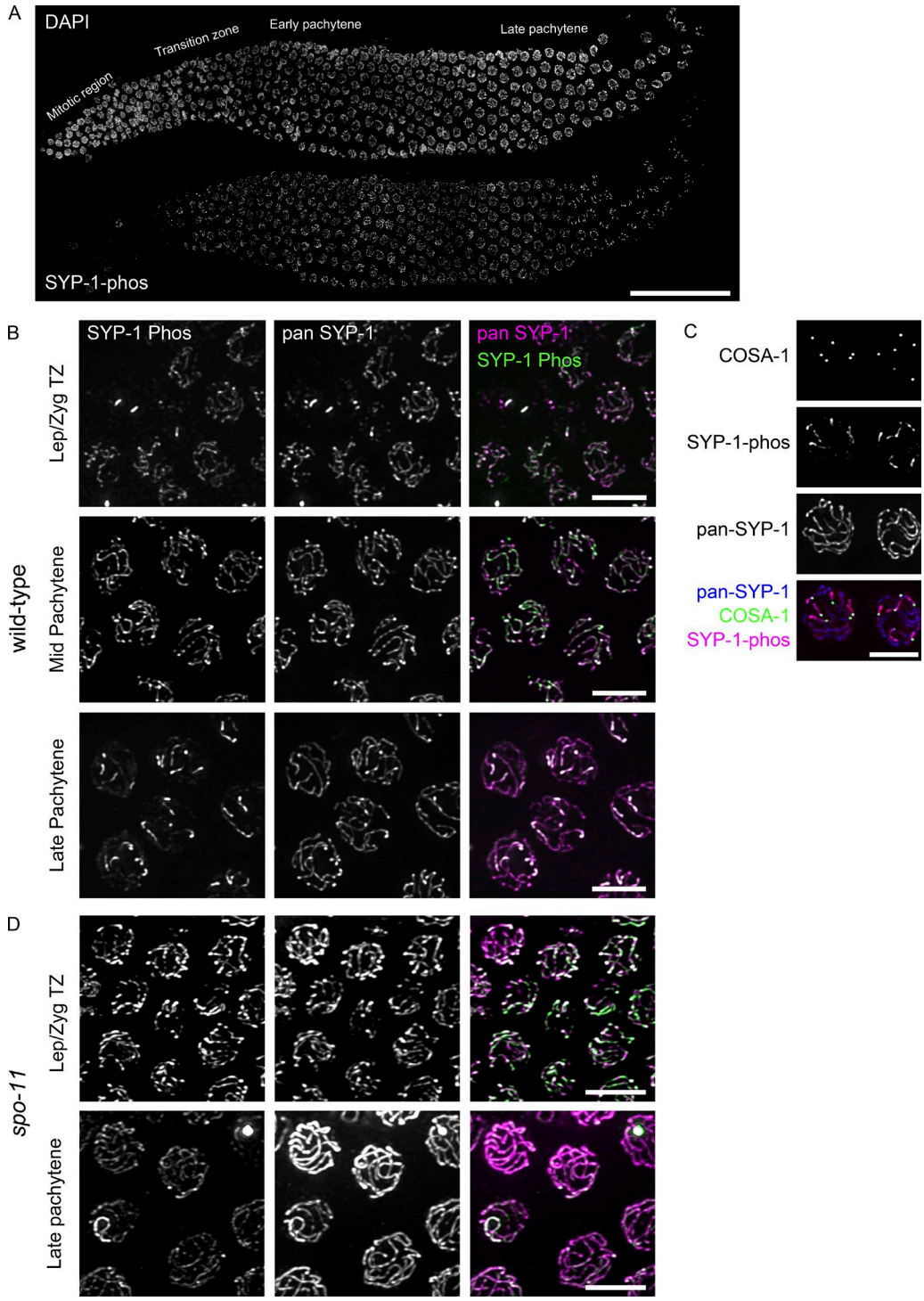

Figure 2. **Phosphorylated SYP-1 localizes to the entire SC in early prophase and then becomes progressively restricted to the short arm. (A)** A wild-type gonad stained with DAPI (top) and antibodies against phosphorylated SYP-1 (bottom). Bar, 50 µm. **(B)** High-magnification images of SYP-1-phos (green) and pan-SYP-1 (magenta) staining from the indicated gonad regions showing SYP-1-phos on chromosomal subdomains in late pachytene. Bars, 5 µm. **(C)** Short arm restriction of SYP-1-phos (magenta) in late pachytene nuclei shown by GFP::COSA-1(green) marking of CO designation sites; pan-SYP-1 is shown in blue. Bar, 5 µm. **(D)** SYP-1-phos and pan-SYP-1 staining in *spo-11 (me44)* mutant gonads. Bars, 5 µm.

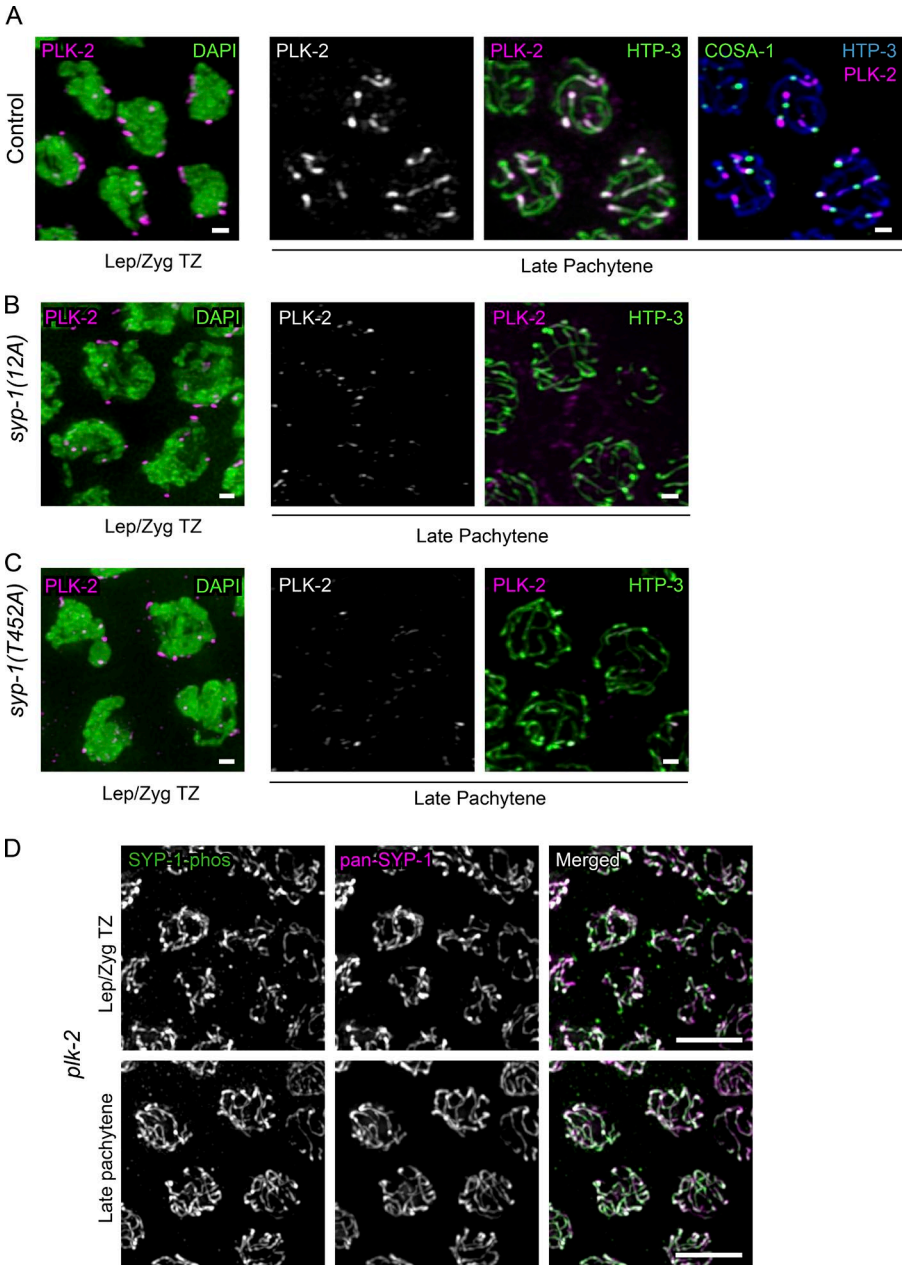

Figure 3. **Phosphorylation of SYP-1 at Thr452 (PBD-binding motif) is required for PLK-2 relocalization from the PC to the SC.** **(A)** Left: Wild-type (N2) oocyte precursor cells in the leptotene/zygotene TZ immunostained with DAPI (green) and PLK-2 (magenta); *right:* oocyte precursor cells in late pachytene in control *gfp::cosa-1* animals immunostained with PLK-2 (magenta) and HTP-3 (green), or PLK-2 (magenta), HTP-3 (cyan) and COSA-1::GFP (green) in the rightmost column. **(B)** As in A, but for *syp-1(12A); syp-1(me17)* mutants, and without COSA-1 staining. **(C)** As in B, but for *syp-1(T452A) syp-1(me17)* mutants. Immunostaining shows PLK-2 relocalization from PCs to the SC (short arms) in control animals, but not in the *syp-1* mutants. Bars, 1 µm. **(D)** SYP-1-phos and pan-SYP-1 localization in *plk-2(ok1936)* mutant gonads. Bars, 5 µm. In all images, color of text label indicates color of the corresponding signal in merged images.

back loop wherein PLK-2 is required to confine SYP-1-phos to short arms in response to CO designation, and SYP-1-phos in turn restricts PLK-2 itself to short arms.

SYP-1 phosphorylation is required for correct timing of early meiotic prophase events

To gain insight into the chromosome segregation defects in 12A mutants, we next examined earlier steps in meiosis: chromosome pairing, synapsis, recombination, and CO designation. Homologous chromosome pairing was assessed by staining of ZIM proteins (Phillips and Dernburg, 2006) binding the PC of chromosomes I and IV (ZIM-3) or V (ZIM-2). When chromosomes are fully homologously paired, the protein ZIM-3, which binds the PCs of chromosomes I and IV, is seen as two foci, whereas ZIM-2, binding to chromosome V, shows a single focus per nucleus. Chromosome pairing at these sites was found to be normal in *syp-1*(12A) mutants (Fig. S2 A and not depicted). Next, we assessed chromosome synapsis by immunofluorescence against the SC proteins. Immunostaining showed that SYP-1(12A) protein colocalized with the axial element protein HTP-3, indicating that the nonphosphorylatable protein is expressed and correctly localized similarly to wild-type SC (Fig. 4, A and B). However, in *syp-1*(12A) and *syp-1(T452A)* mutants, we often observed unsynapsed chromosomes, which are positive for HTP-3 staining but missing SYP-1, in nuclei from the region corresponding to wild-type mid and late pachytene (Fig. 4, B and C). In contrast to *12A* and *T452A* mutants, we detected neither delayed nor partial synapsis in *10A* mutants (Fig. 4 D). This suggests that SYP-1 phosphorylation at the PBD-binding motif is necessary to promote timely and complete SC formation.

We next examined the timing of progression through meiotic prophase in *syp-1* phosphorylation mutants by measuring the proportion of the gonad occupied by each substage. Meiotic nuclei move unidirectionally through the *C. elegans* gonad in a

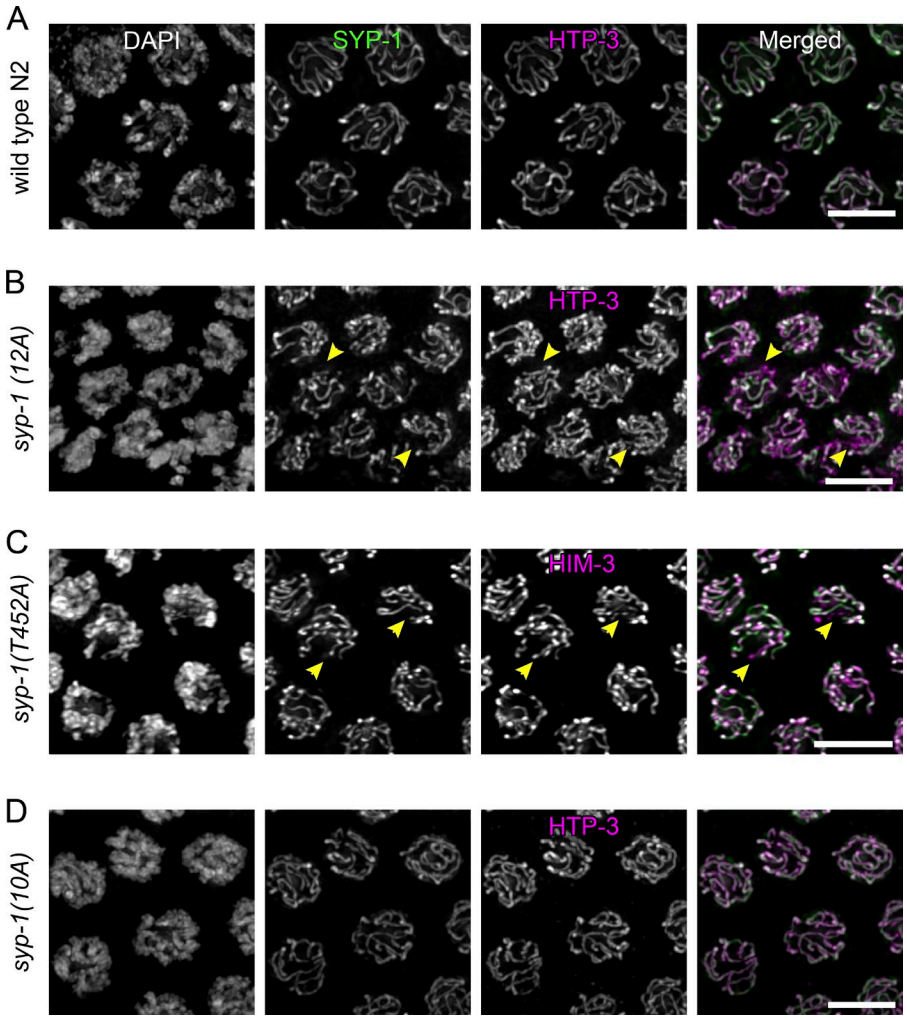

Figure 4. **Phosphorylation of SYP-1 is required for timely completion of synapsis. (A–D)** Oocyte precursor cells in mid-pachytene immunostained with SYP-1 and HTP-3 antibodies in wild-type (A), *syp-1(12A); syp-1(me17)* (B), *syp-1(T452A); syp-1(me17)* (C), and *syp-1(10A); syp-1(me17)* (D) animals. DNA is counterstained with DAPI. Unsynapsed chromosomes in 12A and T452A mutants are indicated by arrowheads. Bars, 5 µm.

manner that allows the physical span of a substage to serve as a proxy for its duration (Hirsh et al., 1976; Jaramillo-Lambert et al., 2007). We found that gonads of both *syp-1(12A)* and *syp-1(10A)* mutants showed delayed exit from the leptotene/zygotene TZ and early pachytene stages compared with control animals (Fig. 5, A and B; and Fig. S2, B and C). Previous studies have shown that meiotic checkpoints monitor the formation of CO intermediates and the status of synapsis (Bhalla and Dernburg, 2005; Carlton et al., 2006; Saito et al., 2012; Rosu et al., 2013; Stamper et al., 2013; Kim et al., 2015), extending the time spent in the TZ and early pachytene for nuclei lacking CO intermediates. When chromosomes fail to obtain CO intermediates, the cell cycle checkpoint kinase CHK-2 is activated and continues to phosphorylate PC proteins, which keeps PLK-2 bound to PCs (Kim et al., 2015). Subsequently, PC-bound PLK-2 nucleates the SUN-1–ZYG-12 nuclear envelope complex to connect chromosome ends to the cytoskeleton and promotes clustering of chromosomes, a cytological marker for the TZ and early pachytene. (Harper et al., 2011; Labella et al., 2011; Woglar et al., 2013). Gonads from 12A and 10A mutants showed an extended region of the TZ, suggesting that PLK-2 persistence at PCs maintains clustering of chromosomes in these mutants (Fig. 5 A). Gonads from 12A, T452A, and 10A mutants also had an extended early pachytene stage, marked by phosphorylation of the nuclear protein SUN-1 (SUN-1 Ser8-phos; Penkner et al., 2009; Figs. 5 B and S2 D; T452A is not depicted). Delayed exit from early pachytene could be explained by the complete or partial inability of PLK-2 to transit from PCs to the SC. In addition, delayed synapsis leading to delayed formation of COs in 12A and T452A mutants would activate the CHK-2–mediated meiotic checkpoint (Kim et al., 2015), which promotes retention of PLK-2 by continuous phosphorylation of PC proteins, delaying the exit from early pachytene.

Next, we examined the contribution of SYP-1 phosphorylation to recombination and CO formation by visualizing the recombination protein RAD-51 and formation of intact bivalents. RAD-51 foci appeared with normal timing in *syp-1(12A)* and *syp-1(10A)* mutants, suggesting that the initiation of programmed DNA DSBs by SPO-11 is not perturbed in these mutants. Instead, the number of RAD-51 foci per nucleus was found to be prominently increased in mid and late pachytene (zones 4–7) in 12A and less prominently increased in 10A mutants compared with control animals (Fig. 5 C). In 12A mutants, delayed synapsis would be expected to lead to delayed homologous recombination and activate the CHK-2–mediated meiotic checkpoint, extending the window during which DSBs are generated. In contrast, 10A mutants had increased levels of DSBs without obvious delays in synapsis. This suggests that persistence of PLK-2 at PCs (or absence of PLK-2 from the SC) could suffice to maintain the DSB-generating machinery in an active state with or without activating the upstream kinase CHK-2. In addition, recent results show that PLK-1/2–

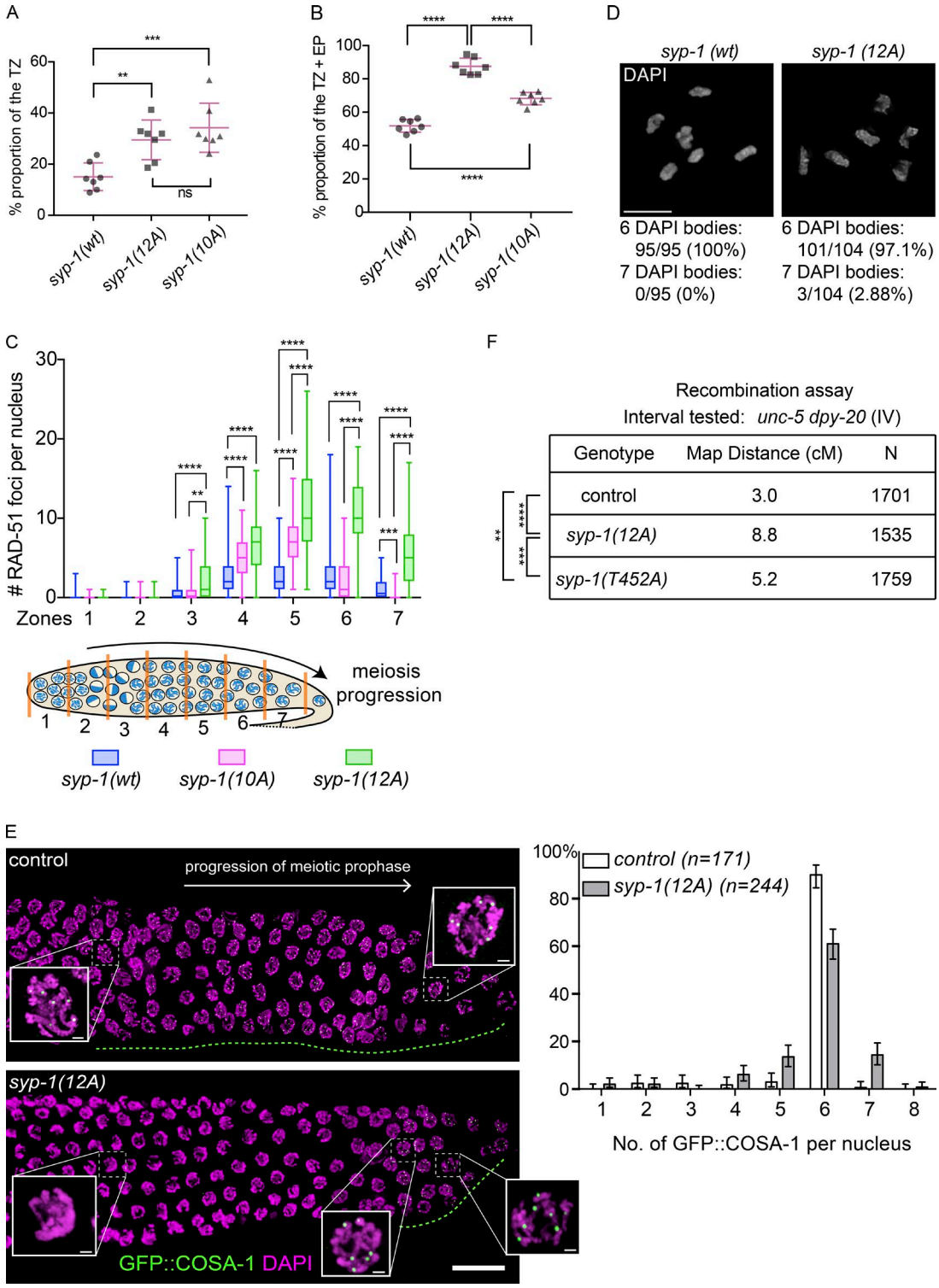

Figure 5. **Phosphorylation of SYP-1 is required for timely progression through meiotic prophase and affects CO distribution. (A)** The proportion of TZ nuclei in *syp-1(wt); syp-1(me17)*, *syp-1(12A); syp-1(me17)*, and *syp-1(10A); syp-1(me17)* animals (see also Materials and methods and Fig. S2). Seven gonads were scored for each genotype. Error bars show SD. Statistical analysis was performed with a Mann–Whitney test (**, P < 0.01; ***, P < 0.001). **(B)** The proportion of TZ and early pachytene nuclei marked by SUN-1 Ser8-phos staining. Error bars show SD. Seven gonads were scored for each genotype. ****, P < 0.0001, Mann–Whitney test. **(C)** Quantification of recombination marker RAD-51 focus counts in each of seven equal-length zones covering the TZ to late pachytene. RAD-51 focus numbers per nucleus are depicted as a box plot, with box indicating mean and quartiles, and whiskers indicating the entire range of measurements. Four gonads were scored for each genotype. The *syp-1(12A); syp-1(me17)* and *syp-1(10A); syp-1(me17)* mutants showed increased levels of RAD-51 compared with the control *syp-1(wt); syp-1(me17)*. ****, P < 0.0001; ***, P < 0.001; **, P < 0.01, Mann-Whitney test. **(D)** Representative diakinesis chromosomes from *syp-1(wt); syp-1(me17)* (left) and *syp-1(12A); syp-1(me17)* mutant (right) gonads stained with DAPI. Statistics of DAPI body observations are shown below. A total of 95 nuclei were scored for the control and 104 nuclei scored for 12A mutants. Bars, 5 µm. (E, left) The timing of appearance of the CO designation marker GFP::COSA-1 is delayed in *syp-1(12A); syp-1(me17)* mutants. The direction of meiotic prophase progression is from left to right. The gonad region in which GFP::COSA-1 foci (green) are observed is highlighted with a green dotted line for

mediated phosphorylation of SYP-4 is required to turn off DSB formation (Nadarajan et al., 2017). To test whether SYP-1 phosphorylation is required for SYP-4 phosphorylation, we immunostained *syp-1* phosphomutants and found that SYP-4-phos signals are still detected (Fig. S2 F) in both 12A and T452A mutants. This suggests that the increase in RAD-51 focus numbers we observe in *syp-1(12A)* is not solely caused by loss of SYP-4 phosphorylation.

To investigate whether the increase in recombination intermediates in 12A mutants could explain the observed meiotic chromosome segregation defects and 40% reduction in progeny viability as a consequence of incomplete recombination, we next examined bivalent formation in diakinesis by scoring the number of DAPI-staining bodies in late meiotic prophase. We found that 12A mutants form meiotic bivalents held together by chiasmata at nearly wild-type levels (97.1%, $n = 104$; Fig. 5 D). The fraction of diakinesis nuclei with univalents (chromosomes lacking COs) in 12A mutants was 2.9% (7 DAPI bodies: 5 bivalents and 2 univalents, $n = 104$), whereas it was 0% in the wild type ($n = 95$). We further examined DAPI-staining bodies for the presence of intra- and interbivalent DNA bridges, morphological features suggestive of improperly resolved recombination intermediates (Saito et al., 2013). We found one intrabivalent bridge out of 31 (3.2%) examined nuclei in *syp-1(12A)* and one interbivalent bridge out of 11 (9.1%) examined nuclei in *syp-1(T452A)* compared with none in 48 wild-type nuclei (0%). This suggests although *syp-1* phosphomutants show delayed meiotic progression, a relatively minor fraction of meiocytes suffer from improperly resolved or unrepaired recombination.

SYP-1 phosphorylation affects CO distribution

Previous studies have shown that SYP-1 is required for CO distribution and designation along chromosomes (Hayashi et al., 2010; Libuda et al., 2013). We tested whether SYP-1 phosphorylation affects the timing and extent of CO designation by visualizing COSA-1 in late pachytene. Meiotic nuclei which obtain DSBs in mid pachytene acquire competence to load COSA-1 at eventual CO sites (Yokoo et al., 2012). We observed a significant delay in COSA-1 appearance in 12A mutants, consistent with the observation that the TZ and early pachytene are extended and meiotic cell cycle progression is delayed. In control animals, sites marked by GFP::COSA-1 foci start to appear in late pachytene, which corresponds to ∼40% of the meiotic region of the gonad (the last 40% of the proximal end). In contrast, 12A mutants showed GFP::COSA-1 foci appearing only at the very end of the gonad (last 10% of the proximal end), where meiotic nuclei finally exit early pachytene and show late pachytene chromosome morphology (Figs. 5 E and S2 E). In contrast to 12A mutants, 10A mutants showed wild-type timing of GFP::COSA-1 foci appearance (Fig. S2 E), indicating that entrance into late pachytene is not delayed in 10A mutants. Immunofluorescence of 10A mutant gonads suggests that although the TZ and early pachytene (marked by SUN-1 Ser8-phos) are prolonged in 10A mutants, entrance into late pachytene (marked by GFP::COSA-1) is not delayed, because of a compensatory loss of mid pachytene (marked by neither; unpublished data). Quantitation of GFP::COSA-1 foci revealed an increased fraction of nuclei with 7 COSA-1 foci in 12A mutants (14.3% in 12A compared with 0.6% in control), suggesting that CO designation is perturbed in the absence of SYP-1 phosphorylation. Although we detected a slightly increased number of nuclei with only five GFP::COSA-1 foci in 12A (13.3% in 12A compared with 2.9% in control), eventual completion of a sixth CO or apoptotic culling would result in a lower frequency of diakinesis nuclei with univalents, as we observe. To further assess the extent of CO recombination in *syp-1* phospho mutants, we measured the genetic distance between the *unc-5* and *dpy-20* genes on chromosome IV. In control animals, the distance was calculated as 3.0 cM, in agreement with the reference map distance of 3.44 cM (WormBase WS260). However, the 12A and T452A alleles showed significantly larger distances (Fig. 5 F), suggesting either an elevated CO frequency or changes in the recombination landscape. Interestingly, the map distance measured in 12A mutants (8.8 cM) was also significantly larger than that in T452A mutants (5.2 cM), raising the possibility that the different levels of SYP-1 phosphorylation might influence CO designation capacity differently. These experiments show that loss of SYP-1 phosphorylation alters levels of synapsis and recombination as well as CO designation and distribution, which together are likely to partially contribute to the inviability observed in the *syp-1* phosphomutants.

SYP-1 phosphorylation promotes establishment of short/long arm asymmetry

Previous studies have shown that PLK-2 plays essential roles in the establishment of short and long arm asymmetry in addition to its role in homologue pairing and synapsis (Harper et al., 2011; Labella et al., 2011; Nadarajan et al., 2017; Pattabiraman et al., 2017). The observed confinement of SYP-1-phos signals to short arms also raises the possibility that SYP-1 phosphorylation is involved in the functional distinction of the short and long arms. To test this hypothesis, we used immunofluorescence to examine protein localization on diakinesis chromosomes. Wild-type SYP-1 departs from long arms as bivalents undergo diplotene remodeling (Fig. 6 A) and eventually departs from short arms no later than the −3 oocyte (Fig. S3). In contrast, we found that nonphosphorylatable SYP-1, as well as SYP-2, always persists on both the short and long arms of diakinesis chromosomes until the −2 or −1 oocyte in the *syp-1(12A)* or *(T452A)* mutants (Fig. 6, B and C; and Fig. S3 D; SYP-2 is not depicted). This result shows that phosphorylation of SYP-1 is required for its timely removal from long and short arms. We next visualized proteins reported to dissociate from the short arm after CO formation: HTP-1/2, LAB-1, and COH-3/4 (de Carvalho et al., 2008; Martinez-Perez et al., 2008; Severson and Meyer, 2014). These proteins also remained on both short and long arms on at least one chromosome in the majority of

the control *gfp::cosa-1* and *syp-1(12A) gfp::cosa-1; syp-1(me17)* gonads. DNA is counterstained by DAPI (magenta). **(E)** Right: quantitation of COSA-1 focus numbers from three gonads for the control *gfp::cosa-1* or ten gonads for *syp-1(12A) gfp::cosa-1; syp-1(me17)* mutants ($n = 171$ nuclei scored for wild type, 244 nuclei scored for *syp-1(12A)*). Bar heights are percentages of nuclei with the given number of COSA-1 foci; error bars show 95% confidence intervals. Bars: (main) 15 µm; (insets) 1 µm. **(F)** Measured genetic map distances in centimorgans for the interval *unc-5—dpy-20* on chromosome IV scored on the given number (N) of *unc-5 dpy-20/+ +* (control), *syp-1(12A); unc-5 dpy-20/+ +; syp-1(me17),* and *syp-1(T452A); unc-5 dpy-20/++; syp-1(me17)* self-progeny. ****, $P < 0.0001$; ***, $P = 0.0001484$; **, $P = 0.001336$, Fisher's exact test.

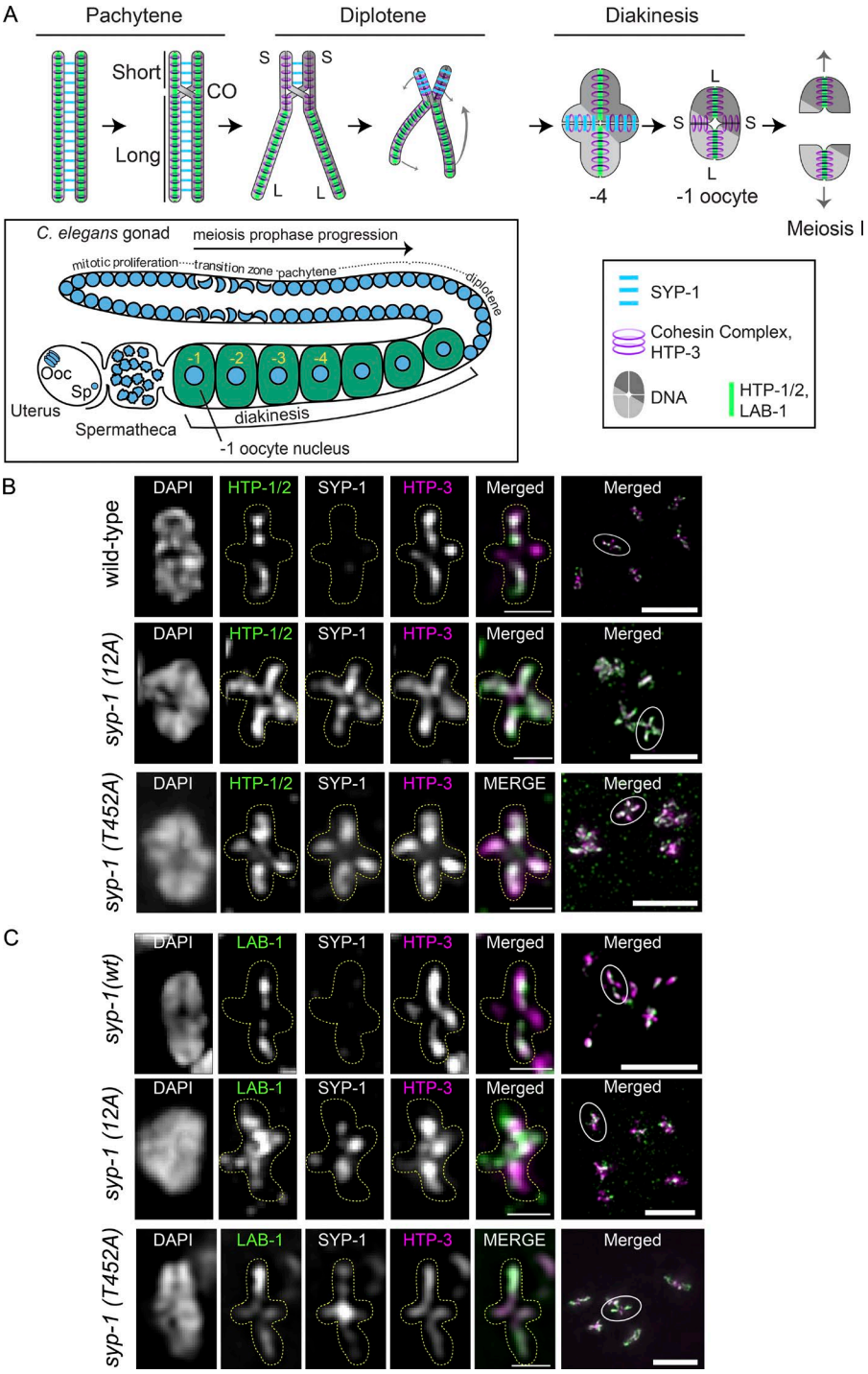

Figure 6. **Phosphorylation of SYP-1 is required for the asymmetric localization of factors involved in chromosome segregation. (A)** Top: Diagram of chromosome axis remodeling during meiotic prophase from pachytene through meiosis I. Cruciform axis of HTP-3/cohesin with short arm (S) and long arm (L) is shown in diakinesis. Bottom: Diagram of meiotic prophase substages in the *C. elegans* gonad with meiotic nuclei indicated by blue circles. Ooc, oocyte nucleus; Sp, sperm pronucleus. Diakinesis nuclei are referred to by their position relative to the spermatheca, with the nearest diakinesis nucleus being the −1 oocyte. After entering the spermatheca and becoming fertilized, the −1 oocyte nucleus goes through the meiosis I and II divisions to generate the oocyte pronucleus. **(B and C)** Partial Z-projection images of a representative chromosome pair in −1 or −2 oocytes with immunostaining for HTP-1/2 (green), SYP-1, and HTP-3 (magenta; B) or LAB-1 (green), SYP-1, and HTP-3 (magenta; C) in the *syp-1(wt); syp-1(me17)* (−1 oocyte), *syp-1*(12A)*; syp-1(me17)* (−1 oocyte), and *syp-1(T452A); syp-1(me17)* (−2 oocyte) gonads. The 12A and T452A mutant gonad shows aberrant persistence of SYP-1 on both arms (see also Fig. S3 D), and HTP-1/2 and LAB-1 on short arms, in −1 or −2 oocytes. In B and C, representative chromosomes are presented with the color of image label indicating the color of immunostaining in the merged image. Full-projection images of each nucleus are shown in the rightmost column, with the chromosome pair shown on the left encircled. The cruciform axis of HTP-3 is visible only for chromosomes lying perpendicular to the optical axis. Bars: (magnified insets) 1 µm; (full projection images at right) 5 µm.

−1 oocytes in *syp-1*(12A) and *syp-1*(T452A) mutants (Fig. 6, B and C; and Fig. S3 A). These results indicate that C-terminal phosphorylation of SYP-1 promotes the establishment of short/long chromosome arm asymmetry, as well as the timely disassembly of SYP-1 from the SC.

To further understand the function of SYP-1 phosphorylation, we created alleles with all 12 phosphosites mutated to D or E (12D or 12E), an alteration that in some cases mimics phosphorylation. However, we found that viability, male progeny production, and immunostaining phenotypes of *syp-1(12E)* and *syp-1(12D)* were indistinguishable from *syp-1(12A)*, with SYP-1 persisting on both short and long arms in diakinesis (Fig. S2 C and Fig. S3, B–D). From this, we conclude that SYP-1(12D) or (12E) may functionally resemble the nonphosphorylatable 12A alleles rather than mimicking constitutively phosphorylated SYP-1.

The CPC is mislocalized in syp-1 nonphos mutants

The arm asymmetry defects and anaphase bridges we observed in *syp-1(12A)* mutants next prompted us to examine the localization of the CPC. Loss of arm asymmetry caused by *laboratory-1* or *htp-1* mutations has been linked to mislocalization of AIR-2 (Aurora B) and the CPC, of which AIR-2 (Aurora B) is a part, leading to chromosome segregation defects (de

Carvalho et al., 2008; Martinez-Perez et al., 2008). To examine whether *syp-1(12A)* mutations lead to CPC mislocalization, we looked at −1 oocytes of 12A mutants. In control animals expressing GFP::AIR-2, we observed the expected concentration of AIR-2 (Aurora B) on short arms in −1 oocytes, followed by its localization to the meiotic spindle in anaphase I and relocalization between sister chromatids at metaphase II. In contrast, in *syp-1*(12A) mutants, AIR-2 (Aurora B) was faint and disorganized in many of the corresponding oocytes, as well as on chromosomes in metaphase/anaphase I (Fig. 7 A). Similarly, the CPC component INCENP (ICP-1 in *C. elegans*) shows robust localization to short arms in wild-type −1 oocyte nuclei, whereas *syp-1(12*A) and *syp-1 (T452A)* mutants had significantly reduced levels of ICP-1 signals in the corresponding nuclei: 81% of nuclei showed reduced ICP-1 signals compared with the wild type, whereas 19% of nuclei showed no ICP-1 signal on any chromosomes in 12A mutants (Figs. 7 B and S4). In *plk-2* mutants, an even stronger loss of ICP-1 from short arms was observed in −1 oocytes: 40% of nuclei showed reduced ICP-1 signals compared with the wild type, whereas 60% of nuclei showed no ICP-1 staining on any chromosomes. We noted that the magnitude of ICP-1 reduction does not correspond to the level of progeny viability in *syp-1(12A)* (60% viability) or *plk-2 (ok1936)* (34% viability; Harper et al., 2011) mutants. Further examination revealed that although wild-type gonads always show ICP-1 signals on short arms from the −3 or −4 oocyte stage, some of the *syp-1(12A)* and *plk-2 (ok1936)* mutant gonads have ICP-1 signals on prometaphase I chromosomes, but not diakinesis chromosomes (Fig. S4 A [*plk-2*]; 12A is not depicted). This suggests that ICP-1 is sometimes capable of rapidly accumulating on chromosomes upon entrance to the meiosis I division without significant prior accumulation in prophase. This is likely a result of redundant positive feedback mechanisms that enhance CPC localization (Carmena et al., 2012) and could partially explain the significant progeny viability observed in *syp-1(12A)* and *plk-2 (ok1936)* mutants. Consistent with reduced localization of the CPC in *syp-1(12A)* mutants, levels of H3Ser10 phosphorylation, which is mediated by AIR-2 (Aurora B) kinase (Hsu et al., 2000), were also reduced in *syp-1(12A)* mutants compared with the wild type (Fig. S4 D). The mislocalization of the CPC could lead to failures in triggering cohesin cleavage and the spindle assembly checkpoint and could explain the anaphase chromosome bridges and loss of viability found in *syp-1*(12A) mutants.

Because LAB-1 has been shown to promote the phosphatase activity of GSP-2 (PP1) at the SC in wild-type animals (Tzur et al., 2012), and because we observed mislocalization of LAB-1 and the CPC in *syp-1(12A)* mutants, we next examined the localization of phosphorylated H3T3, which has been shown to recruit the CPC and is a substrate of PP1 in other model organisms (Qian et al., 2011). In wild-type germlines, H3T3ph signals appeared on the short arm of diakinesis chromosomes from the −3 to −4 oocyte stage. In contrast, H3T3ph was strikingly reduced or absent from short arms in −1 oocytes in *syp-1*(12A) mutants (Figs. 7 C and S4 C). This suggests that in 12A mutants, LAB-1 mislocalizes to both long and short arms, promoting dephosphorylation of H3T3 via GSP-2 (PP1) on the entire chromosome.

To confirm that PP1 dephosphorylates H3T3ph in *C. elegans* meiosis, we immunostained H3T3ph in worms homozygous for the *gsp-2*(PP1) deletion allele *tm301*. In contrast to the short arm–specific H3T3ph staining in wild type, *gsp-2*(PP1) mutants showed H3T3 phosphorylation over the entire chromosome from diakinesis onward (Fig. 8 A). This suggests that dephosphorylation of H3T3 by PP1 is likely to be conserved in *C. elegans*. Similarly to H3T3ph staining, ICP-1 was present all over chromosomes in *gsp-2 (PP1)* mutants by immunofluorescence (Fig. 8 B).

Collectively, the high incidence of defects in the asymmetric disassembly of SC components and compromised CPC localization likely explain the bulk of reduced viability in *syp-1(12A)* and *(T452A)* mutants by causing chromosome segregation problems at meiosis I. The loss of short/long arm asymmetry in the nonphosphorylatable SYP-1 alleles and the dynamic localization of SYP-1-phos signals are two independent lines of evidence that strongly suggest that phosphorylation of SYP-1 is a key element of the molecular cascade that establishes domains of successive cohesion loss de novo in response to COs.

Discussion

Here, we have shown that phosphorylation of SYP-1 at its PBD-binding motif promotes timely synapsis and progression of meiotic prophase, affects recombination rates, and is critical for early steps in establishing the short and long arm chromosome domains essential for correct meiotic disjunction. SYP-1 phosphorylation begins at the TZ as SYP-1 proteins polymerize between axial elements. Once COs are made and meiocytes enter the late pachytene stage, phosphorylated SYP-1 and PLK-2 localize to short arms and vacate the long arms. This asymmetric distribution is required for the full establishment of functionally distinct short and long arms in diplotene and diakinesis. Prevention of SYP-1 phosphorylation at its PBD-binding motif disrupts PLK-2 relocation from PCs to the SC, delays synapsis and CO formation, and delays the exit from the TZ and early pachytene. Without SYP-1 phosphorylation, meiotic defects from early and late prophase lead to mislocalization of the CPC, resulting in chromosome missegregation and reduced progeny viability. Collectively, our results suggest that PLK-2 acts through SYP-1 (potentially through SYP-1's PBD-binding motif) to ensure confinement of the chromosome segregation machinery to the short arm subdomain, promoting correct segregation of holocentric chromosomes in meiosis I.

PLK-2 has been shown to bind to PC proteins at nuclear envelope-associated LINC complexes to promote chromosome pairing and synapsis in the TZ (Harper et al., 2011; Labella et al., 2011). Our results raise the possibility that SYP-1 protein phosphorylated at its PBD-binding motif in the nascent SC could provide a new binding site for PLK-2. This new site could promote meiotic events in two ways: (1) by allowing PLK-2 to move off of PCs (possibly in cis), promoting the progression of the cell cycle, and (2) by recruiting PLK-2 to the SC to establish short and long arm distinction. PLK-2 bound to SYP-1-phos could then phosphorylate other proteins in the vicinity of the SC, initiating a phosphorylation cascade.

Phosphorylated SYP-1 localizes to the short arm immediately after COSA-1 focus formation in late pachytene, suggesting that this relocation is one of the earliest events to take place after recombination intermediates are committed to COs. Another SC central component, SYP-3, has been shown to dynamically move onto and off of chromosomes during meiotic prophase. In a process dependent on PLK-2, this exchange

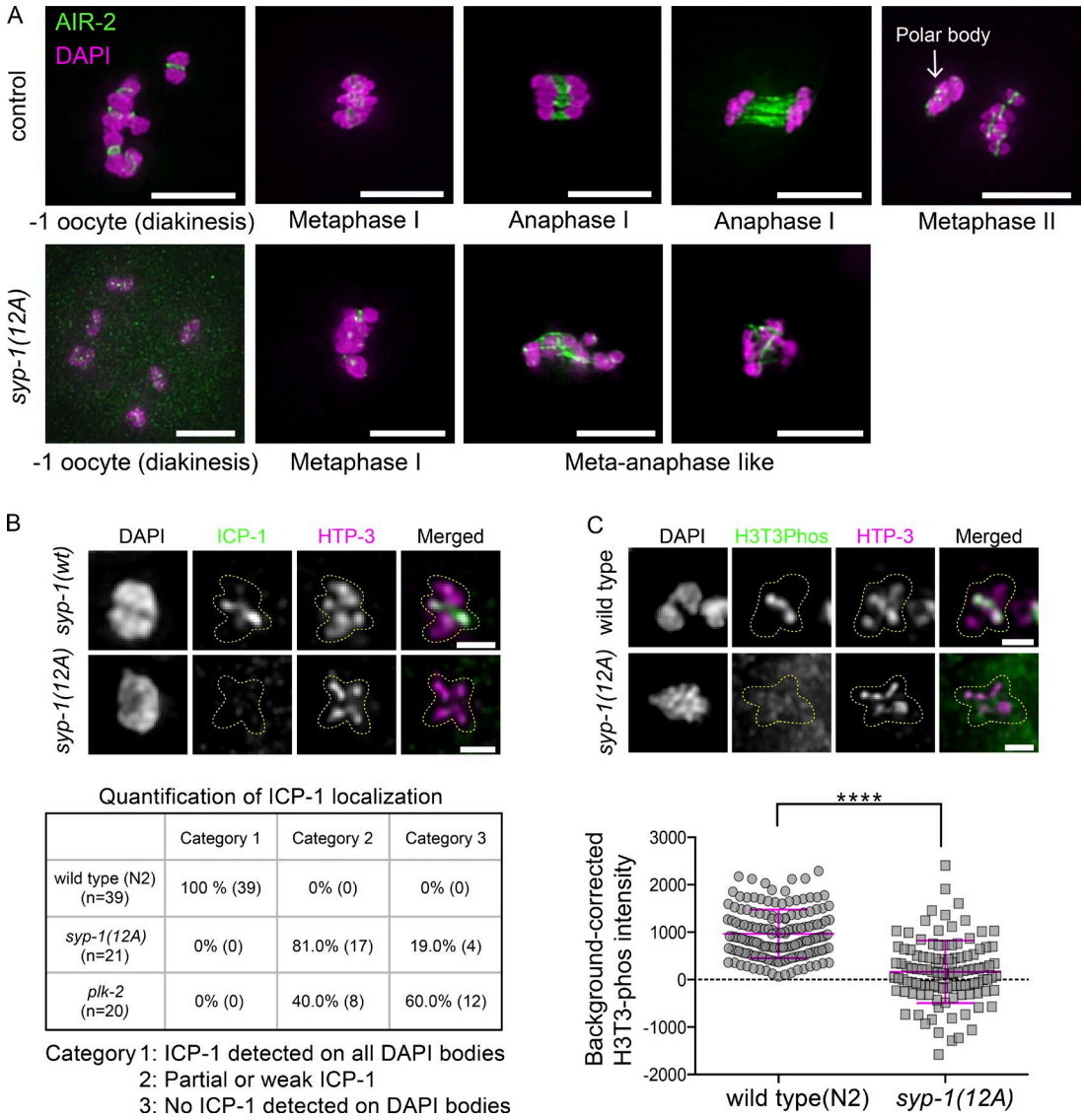

	Category 1	Category 2	Category 3
wild type (N2) (n=39)	100 % (39)	0% (0)	0% (0)
syp-1(12A) (n=21)	0% (0)	81.0% (17)	19.0% (4)
plk-2 (n=20)	0% (0)	40.0% (8)	60.0% (12)

Figure 7. **SYP-1 phosphorylation is required for correct localization of CPC components (AIR-2 and ICP-1) and the CPC-guiding histone mark (H3T3ph). (A)** Localization of GFP::AIR-2 (green) on meiotic chromosomes fixed and stained with DAPI (magenta) at different stages preceding and during the meiotic divisions in control (*gfp::air-2*)(top) and *gfp::air-2; syp-1(12A); syp-1(me17)* (bottom) animals. Bars, 5 µm. **(B)** ICP-1 is enriched on short arms in −1 oocytes in *syp-1(wt); syp-1(me17)* animals (top), whereas some −1 oocytes lack ICP-1 localization in *syp-1(12A); syp-1(me17)* mutants (bottom; see also the whole-nucleus image in Fig. S4). The ICP-1 localization in −1 oocytes was categorized as follows in *syp-1(wt); syp-1(me17), syp-1(12A); syp-1(me17),* and *plk-2(ok1936)*: all six DAPI bodies had robust ICP-1 staining on short arms (category 1), some DAPI bodies had partial or weak ICP-1 staining (category 2), or no DAPI bodies had ICP-1 staining (category 3). The analysis was limited to −1 oocyte nuclei carrying six bivalents. Bars, 1 µm. **(C)** H3T3ph staining in −1 oocyte nuclei in N2 wild-type (top) and *syp-1(12A); syp-1(me17)* mutants (bottom); representative images are shown above quantitation (see also the whole-nucleus image in Fig. S4). Bars, 1 µm. In the scatterplot below, each point is a measurement of a single DAPI body. Error bars indicate mean and SD of all points. The number of DAPI bodies/points counted for H3T3ph is 151 for wild type and 111 for *syp-1*(12A) mutants. ****, $P < 0.0001$, Mann–Whitney test.

becomes less dynamic after COs are made (Pattabiraman et al., 2017). Thus, the asymmetric relocalization of phosphorylated SYP-1 coincides with a large-scale reduction in the dynamic properties of the SC, raising the possibility that both of these PLK-2–dependent events are mechanistically connected.

The SYP-1 phosphomutants also affected COSA-1 focus number and CO recombination rate. In the 12A allele, COSA-1 foci representing CO designation sites departed from the wild-type number of six per nucleus, with ∼13.5% of nuclei having five foci and 14.3% having seven foci. Perturbation of the SC by partial loss of SYP-1 has been shown to increase COSA-1 number (Hayashi et al., 2010; Libuda et al., 2013); perhaps the alterations in our mutant alleles act in a similar fashion by affecting the level of SYP-1 incorporation or the overall integrity of the SC. In contrast, the genetic distance of the *unc-5—dpy-20* interval on chromosome IV increased by more than a factor of two in 12A mutants. The disagreement between the change in COSA-1 foci and the large increase in the genetic map we observed has several nonexclusive possible explanations, including generation of additional COs not marked by COSA-1, a shift of CO formation to a central position (the *unc-5—dpy-20* interval roughly bounds the central third of chromosome IV), or a bias in recovery of chromosomes with COs in this region in the surviving progeny.

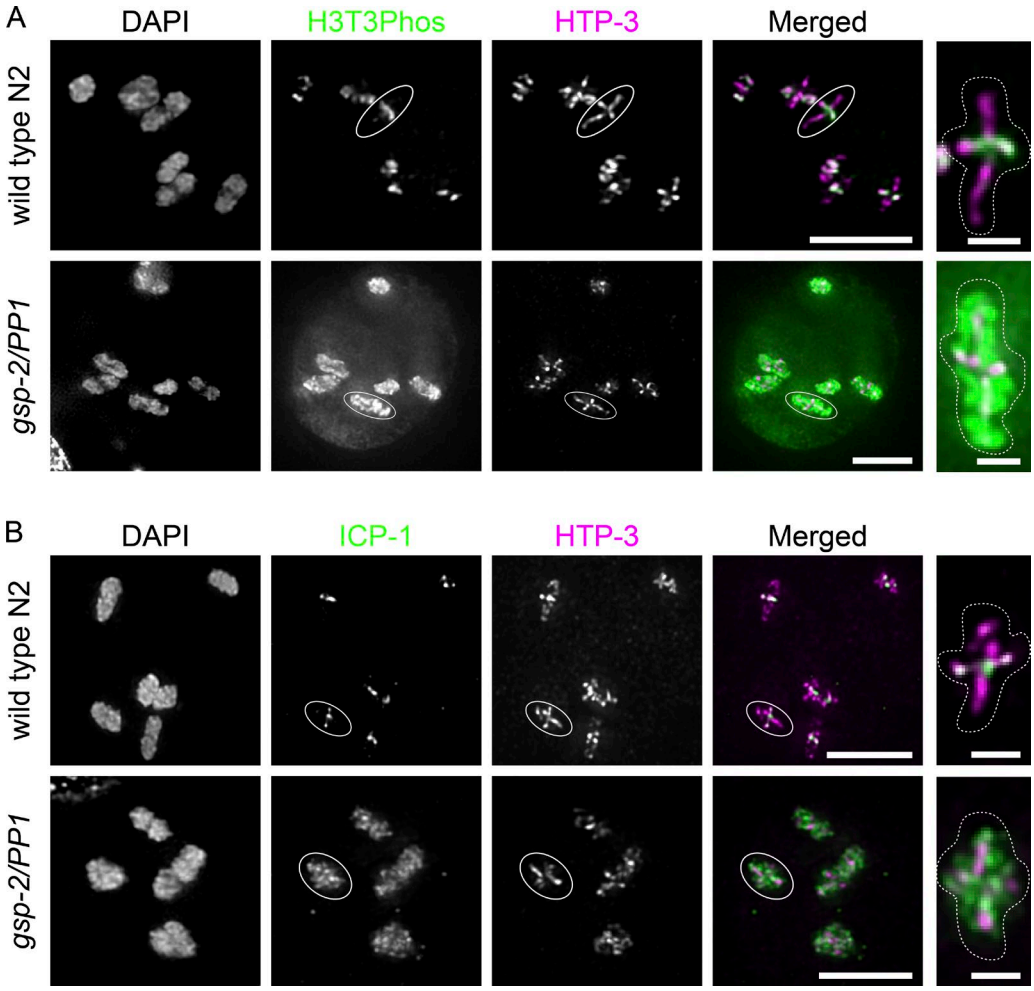

Figure 8. **GSP-2/PP1 restricts the CPC-guiding histone mark H3T3ph and ICP-1 to short arms. (A and B)** H3T3ph immunostaining shown in green (A) or ICP-1 immunostaining shown in green (B) in −1 oocytes in wild type (top) and *gsp-2(tm301)* mutants (bottom). Short and long arms are marked by HTP-3 staining (magenta). Representative chromosomes with cruciform HTP-3 staining indicated by circles are shown in the rightmost panels. Bars: (left) 5 µm; (right) 1 µm.

Loss of SYP-1 phosphorylation nearly always resulted in abnormal persistence of SC or SC-interacting proteins in diplotene and diakinesis, and ICP-1 was never observed at wild type levels in −1 oocytes in *syp-1(12A)* mutants. These very penetrative phenotypes contrast with the relatively high viability (60%) of *syp-1(12A)* mutant self-progeny. If spermatogenesis and oogenesis were equally compromised, this level of viability would suggest that gamete production succeeds at least 77% of the time in the absence of SYP-1 phosphorylation. This would imply that despite the localization defects observed in prophase in *syp-1(12A)* mutants, redundant pathways suffice to deposit CPC components at the short arm by metaphase I in a subset of nuclei. Why some chromosomes in *syp-1(12A)* mutants ultimately succeed in recruiting the CPC to short arms and successfully segregate in meiosis while others do not remains to be determined. One possible explanation is the unpredictable nature of CO position. In *C. elegans*, the obligatory single CO is most likely to occur in the terminal thirds of chromosomes (Barnes et al., 1995). Because establishment of short and long arm domain patterning appears to be determined by the physical distance from the CO to the chromosome ends, perhaps the mechanisms behind this functional distinction could be confounded on chromosomes that happen to receive more centrally located COs. More generally, if COs at different positions (central, arm, or terminal) of chromosomes vary with respect to the ease or speed of subsequent long and short arm domain patterning, then nuclei with an excess of "difficult" COs may be more likely to harbor chromosomes that fail in downstream steps of short and long arm establishment in a sensitized background such as *syp-1(12A)* mutants. Similar reasoning could account for the fact that the *syp-1(10A)* mutant has a slight but significant increase in male production without an increase in embryonic lethality, which suggests the *X* chromosome has a higher nondisjunction rate than autosomes in this mutant. Compared with autosomes, the *X* chromosome has a smaller region of suppressed crossing over near the chromosome midpoint (Rockman and Kruglyak, 2009), predicting a higher incidence of centrally located COs. Such COs, though occurring with low frequency, could result in failure to effectively establish the long and short arm domains in *syp-1(10A)* mutants.

The observation that synapsis is delayed in *syp-1(12A)* or *(T452A)* mutants, but not in *syp-1(10A)* mutants, suggests that SYP-1 phosphorylation at its PBD-binding domain promotes the timely progression of synapsis. Although immunofluorescence against both native and HA-tagged PLK-2 failed to detect PLK-2 on the SC in the TZ or early pachytene in 10A

mutants, a residual amount of PLK-2 at the SC below our detection threshold may suffice to promote timely completion of synapsis in this mutant. However, the fact that many chromosomes achieve timely synapsis even in *plk-2* mutants shows that PLK-2 is not strictly necessary for synapsis. The mechanism of synapsis facilitation by PLK-2 remains unknown but could involve distributive phosphorylation of SC components, which may alter SC structure or binding affinity. In addition to containing the PBD-binding motif, the C terminus of SYP-1 interacts with SYP-3 (Schild-Prüfert et al., 2011), raising the further possibility that phosphorylation of SYP-1 at T452 may modulate its binding capacity to SYP-3 and promote assembly of central components.

How could the localization of phosphorylated SYP-1 on the short arm lead to subsequent localization of the CPC on the same domain at the end of meiotic prophase? Our data show that SYP-1 phosphorylation controls the correct distribution of one of the CPC-guiding histone modifications, phosphorylated histone H3T3. We have shown that SYP-1 phosphorylation is critical for LAB-1 restriction to the long arms, where it normally locally increases the activity of PP1 (Tzur et al., 2012), which we have shown to counteract H3T3 phosphorylation. A previous study in fission yeast demonstrated that the H3T3 kinase Haspin is recruited to centromeres by the cohesin regulator Pds5 (Yamagishi et al., 2010). If this mechanism is conserved in *C. elegans*, then we would expect Haspin to be recruited to the axis region of the SC, because cohesins and the *C. elegans* orthologue of Pds5, EVL-14, associate with the lateral elements (Pasierbek et al., 2001; Kim et al., 2014). Although our detection of globally high H3T3ph levels in *gsp-2* mutants shows that PP1 likely suppresses Haspin activity all over chromatin during diakinesis, additional negative reinforcement may be required specifically at the axis region of the long arms where Pds5 may increase the amount of Haspin present. In addition to this potential mechanism of negative regulation on the long arms we describe, previous work has also shown that Haspin is phosphorylated and activated by PLK in *Xenopus laevis* extracts (Ghenoiu et al., 2013). PLK-2 constrained to the SC short arm by phosphorylated SYP-1 could similarly activate Haspin, and subsequently enrich the CPC at short arms, in *C. elegans.* Our findings, combined with previous results, suggest major functions of SYP-1 phosphorylation in guiding the localization of the CPC by suppressing H3T3 phosphorylation on long arms while promoting it on short arms.

Materials and methods

C. elegans strains and conditions

C. elegans strains were grown using standard procedures (Brenner, 1974) at 20°C. Wild-type worms were from the N2 Bristol strain. The following mutations, transgenes, and balancers were used in this study: *me107[plk-2::HA] (I), plk-2(ok1936)/hT2[bli-4(e937) let-?(q782) qIs48](I;III), gsp-2(tm301)/eT1(unc-36)(I;III), meIs8 [Ppie-1::gfp::cosa-1 + unc-119(+)] (II), icmSi44 [Psyp-1::syp-1(T452A) + unc-119(+)](II), icmSi35 [Psyp-1::syp-1(4A) + unc-119(+)](II), icmSi33 [Psyp-1::syp-1(8A) + unc-119(+)](II), icmSi42 [Psyp-1::syp-1(10A) + unc-119(+)](II), icmSi25 [Psyp-1::syp-1(12A) + unc-119(+)] (II), icmSi31 [Psyp-1::syp-1(12E) + unc-119(+)]* line 2 *(II), icmSi32 [Psyp-1::syp-1(12E) + unc-119(+)]* line 3 *(II), icmSi28 [Psyp-1::syp-1(12D) + unc-119(+)](II), icmSi24 [Psyp-1::syp-1(wild type) + unc-119(+)] (II), zim-2 (tm574) (IV), spo-11(me44)/nT1[unc-?(n754) let-?qIs50](IV;V), syp-1(me17)/nT1[unc-?(n754) let-?(m435)] (IV;V), unc-119(ed3) (III); ltIs14[pie-1p::GFP-TEV-STag::air-2 + unc-119(+)], unc-5 (e53), dpy-20(e1282ts) (IV).*

For all mutant analyses, we used homozygous mutant progeny of heterozygous parents.

The *syp-1* phospho mutants were generated using Mos-SCI (Frøkjaer-Jensen et al., 2008) with pCFJ151 plasmids and the strain EG6699. To generate *syp-1 (12A)*, *(12E)*, and *(12D)* mutants, the *syp-1* gene fragments were synthesized with respective mutations by Invitrogen GeneArt Strings and cloned into pCFJ151 using Gibson assembly cloning kit (New England BioLabs). The rest of the *syp-1* phosphomutations were created by either mutating *syp-1 (wt)* or *(12A)* genes cloned in pCFJ151 using PCR-based mutagenesis (for T452A) or by stitching *syp-1 (wt)* and *(12A)* gene fragments by Gibson assembly cloning (for 4A and 8A mutants). The following primer set was used for PCR-based mutagenesis for T452A: forward, 5′-CCATTGATG ACGAGCGCACCACTTACCGCAGCTACtAGACCGTTGAAACGA AC-3′; and reverse, 5′-GTTCGTTTCAACGGTCTaGTAGCTGCG GTAAGTGGTGCGCTCGTCATCAATGG-3′. This complementary primer set introduces an additional synonymous mutation (indicated by a lowercase t in the forward primer/lowercase a in the reverse primer), because we designed this template to function with either Mos-SCI or CRISPR/Cas9, and this synonymous mutation disrupts a potential protospacer adjacent motif (PAM) sequence. At least two transgenic lines were generated for each transgene for mutant phenotype analysis. All *syp-1* transgenes contain the promoter (500 bp upstream of the gene) and the 3′ UTR (97 bp downstream of the gene). The insertion of the *syp-1* transgene was verified by DNA sequencing.

Phosphoproteomics

Wild-type N2 and *pph-4.1(tm1598)/hT2[bli-4(e937) let-?(q782) qIs48]* worms were grown on NGM plates containing 25 µg/ml carbenicillin and 1 mM IPTG spread with HT115 bacteria either carrying an empty RNAi vector (L4440; http://www.addgene.org/1654) or a *pph-4.1*-RNAi plasmid. To generate the *pph-4.1* RNAi plasmid, the 695-bp region spanning the second, third, and fourth exons of *pph-4.1* was amplified from *C. elegans* N2 genomic DNA using primers 5′-GCT CGTGAAATCCTAGC-3′ (forward) and 5′-CGAATAGATAACCGG CTC-3′ (reverse) flanked by Not1 and Nco1 sites and cloned into L4440. First, N2 and *pph-4.1(tm1598)/hT2[bli-4(e937) let-?(q782) qIs48]* worms (P0) synchronized by starvation were transferred to new plates with food, and worms at the L4 larval stage were harvested in M9 + 0.01% Tween buffer, washed three times with M9 + 0.01% Tween buffer, and distributed to either control or *pph-4.1* RNAi plates. Approximately 30 h later, these worms on RNAi plates were harvested in M9 + 0.01% Tween buffer and bleached to collect embryos. Collected F1 embryos were distributed to fresh RNAi plates. At time points when these F1 worms were either 1 or 3 d after L4 stage, half of the F1 plates were exposed to 10 Gy γ-rays to induce DNA damage. 4 h after irradiation, worms were harvested in M9 buffer, washed three times with M9 buffer, and frozen at −80°C. 2 ml pelleted, frozen worms prepared in this manner was thawed and dissolved in 5 ml urea lysis buffer (20 mM Hepes, pH 8.0, 9 M urea, 1 mM sodium orthovanadate, 2.5 mM sodium pyrophosphate, and 1 mM β-glycerol-phosphate), sonicated for 1 min at 30-s intervals 10 times until worm bodies were broken up. The worm lysates were spun down at 20,000 *g* for 15 min, and supernatants were subjected to PTMScan analysis (Cell Signaling Technology); phosphorylated peptides were enriched by phospho-(Ser/Thr) kinase substrate antibody-immobilized protein A beads and analyzed by liquid chromatography–tandem mass spectrometry using an LTQ-Orbitrap-Elite ESI-CID (Thermo Fisher). Phosphoenrichment antibodies were obtained from CST (catalog numbers 9607, 6966,

8139, 8738, 9624, 6967, 5759, 9942, 10001, 9614, 9477, 8134, 2325, 5243, and 3004). Protein assignments were made using Sorcerer. Peptide counts indicated in Table S1 show pooled counts from all conditions of worms (± RNAi, irradiation, or age) used in this assay.

Microscopy, cytology, and antibodies

For all cytological preparations, we followed protocols described previously (Phillips et al., 2009). Images were acquired on a Deltavision personalDV microscope (Applied Precision/GE Healthcare) with a CoolSNAP ES2 camera (Photometrics) at 23°C, using 60× PlanApoN 1.42 NA or 100× UPlanSApo 1.4 NA oil-immersion objectives (Olympus) and immersion oil (LaserLiquid; Cargille) at a refractive index of 1.513. The Z spacing was 0.2 µm, and raw images were subjected to constrained iterative deconvolution followed by subpixel chromatic shift correction using scripted control of the Priism (Chen et al., 1996) software suite (see code chromatic-shift at https://github.com/pmcarlton/deltavisionquant). Image acquisition was performed with the softWoRx suite (Applied Precision/GE Healthcare). Image postprocessing for publication was limited to linear intensity scaling and maximum-intensity projection using OMERO (Burel et al., 2015). The following antibodies used in the present study have been described previously: HTP-1 (Martinez-Perez et al., 2008; provided by E. Martinez-Perez, Imperial College London, London, England, UK), LAB-1 (de Carvalho et al., 2008) and phosphorylated SYP-4 (Nadarajan et al., 2017; provided by M. Colaiacovo, Harvard Medical School, Boston, MA), PLK-2 (Labella et al., 2011; provided by M. Zetka, McGill University, Montreal, Canada), ICP-1 (Oegema et al., 2001; provided by K. Oegema, Ludwig Institute for Cancer Research, San Diego, CA), HIM-8 (Phillips et al., 2005), HTP-3 (MacQueen et al., 2005), SYP-1 (Harper et al., 2011), and ZIM-3 (Phillips and Dernburg, 2006; provided by A. Dernburg, Lawrence Berkeley National Laboratory, Berkeley, CA), SUN-1:Ser8p (Penkner et al., 2009; provided by V. Jantsch, University of Vienna, Vienna, Austria), and COH-3/4 (Severson and Meyer, 2014; provided by A. Severson, Cleveland State University, Cleveland, OH). Antibodies generated for this work were rabbit-SYP-1_1Phos antibodies generated using the phosphopeptide [SAPLMTSpTPLTAATR], rabbit-SYP-1_3Phos antibodies generated using the phosphopeptide [SAPLM(pT)S(pT)PL(pT)AATR] by Eurofins, all used at 1:100 dilution. All the phospho-specific antibodies were affinity purified using the SulfoLink Immobilization kit (44999; Thermo Fisher) using nonphosphorylated and phosphorylated peptides. The following commercial antibodies were used: anti-GFP (1:500 dilution; 12600500; Roche), anti-Histone H3Thr3ph (Phospho-Histone H3 [Thr3; D5G1I] mAb, 1:10,000 dilution; 13576S; Cell Signaling Technology), anti-Histone H3Ser10Phos (39254, 1:1,000 dilution), rabbit RAD-51 antibody from SDIX/Novus Biologicals (1:1,000 dilution; #29480002, lot# G3048-009A02; Active Motif), rabbit anti-HIM-3 antibody (1:500 dilution; 53470002; SDIX/Novus), anti-HA (1:500 dilution; 901501; Covance/BioLegend), and anti–ZIM-2 (1:500 dilution; 49270002; SDIX/Novus). Secondary antibodies used were DyLight488, DyLight594, DyLight649, or Alexa Fluor 488–conjugated AffiniPure antibodies (1:500 dilution; Jackson ImmunoResearch). All immunofluorescence was performed on adult worms at 1 d after L4.

For H3T3 phosphorylation intensity measurements, Fiji (Schindelin et al., 2012) was used to calculate the intensity of H3T3ph on DAPI bodies. Regions of interest were drawn based on DAPI-positive pixels in −1 oocyte nuclei, and the mean H3Thr3ph pixel intensity within regions of interest was measured. To subtract background intensity, background regions were drawn in the same nucleus outside of the DAPI bodies, whose mean pixel intensity was taken as the background intensity. Intensity data were statistically analyzed by the Mann–Whitney test. The number of DAPI bodies counted for H3T3ph is 151 for the wild type and 111 for *syp-1(12A)* mutants. Quantifications of the length of SUN-1 Ser8ph staining as well as the TZ (defined by clustered nuclei without resolvable chromatids) and RAD-51 foci were performed as described previously (Sato-Carlton et al., 2014). For quantification of RAD-51 foci per nucleus, the nuclei on the coverslip-proximal side of four gonads were scored for each genotype. The numbers of nuclei scored for zones 1–7 were 142, 163, 173, 146, 127, 111, and 92 for *wt*; 210, 241, 172, 129, 142, 104, and 104 for *syp-1*(10A); and 154, 144, 86, 75, 83, 79, and 74 for *syp-1*(12A).

Genetic recombination frequencies

Recombination frequencies were calculated as described previously (Zalevsky et al., 1999). *p*, the map distance, is calculated from the fraction *R* of recombinant self-progeny, as $P = 1 - [(1 - 2R)^{0.5}]$. Males of genotype *icmSi25 [Psyp-1::syp-1(12A) + unc-119(+)]*; *syp-1(me17)/nT1[unc-?(n754) let-? qIs50]*, *icmSi44 [Psyp-1::syp-1(T452A) + unc-119(+)]*; *syp-1(me17)/nT1[unc-?(n754) let-? qIs50]* or N2 were crossed with *icmSi25 [Psyp-1::syp-1(12A) + unc-119(+)]; unc-5 (e53), dpy-20(e1282ts); syp-1(me17), icmSi44 [Psyp-1::syp-1(T452A) + unc-119(+)]; unc-5 (e53), dpy-20(e1282ts); syp-1(me17)* or *unc-5 (e53) dpy-20(e1282ts)* hermaphrodites, respectively. Hermaphrodite cross-progeny were picked to single plates, and their progeny were scored for Unc Dpy, wild type, and Unc non-Dpy or Dpy non-Unc recombinants. The assay was performed at 23°C to observe the temperature-sensitive phenotype of *dpy-20(e1282ts)*. We noted that *syp-1(12A); syp-1(me17)* and *syp-1(T452A); syp-1(me17)* animals generate a small population of sick progeny (worms with abnormal morphology such as arrested development, reduced pigment, early death or Unc; 2.3% and 2.1% of total progeny, respectively) and also that *syp-1(12A); syp-1(me17)* animals generate a small number of Dpy progeny (0.4% of total progeny, presumably because of aneuploidy observed in these mutants). The sick progeny observed in 12A or T452A mutants could be falsely scored as Unc non-Dpy animals in the recombination assay, and indeed, we found more Unc non-Dpy animals than Dpy non-Unc in these mutants. Therefore, we limited our analysis to the class of Dpy non-Unc animals to calculate the recombination rate (i.e., multiplied the number of Dpy non-Unc recombinants by two to estimate the true number of recombinants). Because *syp-1(12A); syp-1(me17)* animals were seen to spontaneously generate 0.4% Dpy progeny, we subtracted this percentage from the total number of observed Dpy non-Unc progeny in this cross before calculating.

Statistics

Experiments in Fig. 5 (A–C), Fig. 7 C, and Fig. S2 (B, C, and E) were tested for significance using the unpaired Mann–Whitney *U* test with two-sided p-values. Confidence intervals in Fig. 5 E (95%) were calculated from the binomial distribution using the Clopper–Pearson method. Experiments in Fig. 5 F and Fig. S1 B were tested for significance using Fisher's exact test with two-sided p-values.

Online supplemental material

Fig. S1 shows conservation of the SYP-1 PBD-binding motif among six nematode species and characterizes *syp-1* phospho mutants. Fig. S2 characterizes *syp-1* phospho mutants. Fig. S3 shows aberrant persistence of SYP-1 and cohesin subunits COH-3/4 in diakinesis nuclei in *syp-1(12A)* mutants. Fig. S4 shows mislocalization of CPC components and CPC-related histone marks in *syp-1(12A)* mutants. Table S1 shows tandem mass spectrometry spectra of SYP-1 phosphopeptides.

Acknowledgments

We thank A.F. Dernburg, M.P. Colaiácovo, E. Martinez-Perez, V. Jantsch, A. Villeneuve, A. Woglar, M. Zetka, K. Oegema, and A. Severson for antibodies, strains, and technical assistance; H. Funabiki and S. Ahmed for critical reading and helpful advice; and the rest of the Carlton laboratory members for discussion and technical assistance. We also thank the anonymous reviewers whose comments improved this manuscript scientifically and editorially. We are deeply indebted to Y. Kim and A.F. Dernburg for sharing their unpublished results.

Many nematode strains were also provided by the Caenorhabditis Genetics Center, which is funded by the National Institutes of Health National Center for Research Resources. This work was supported by a Japan Society for the Promotion of Science postdoctoral fellowship to A. Sato-Carlton, and Japan Society for the Promotion of Science KAKENHI grants (24687024 Wakate A and 15H04328 Kiban B to P.M. Carlton, and 15K18477 Wakate B and 17K15064 Wakate B to A. Sato-Carlton). The iCeMS institute was supported by the World Premier International Research Initiative of the Ministry of Education, Culture, Sports, Science and Technology, Japan.

The authors declare no competing financial interests.

Author contributions: A. Sato-Carlton and P.M. Carlton conceived the experiments. A. Sato-Carlton, C. Nakamura-Tabuchi, S. Kazuki Chartrand, and T. Uchino conducted the experiments. A. Sato-Carlton, C. Nakamura-Tabuchi, and P.M. Carlton wrote the manuscript.

Submitted: 30 July 2017
Revised: 12 October 2017
Accepted: 8 November 2017

References

Barnes, T.M., Y. Kohara, A. Coulson, and S. Hekimi. 1995. Meiotic recombination, noncoding DNA and genomic organization in Caenorhabditis elegans. *Genetics.* 141:159–179.

Bhalla, N., and A.F. Dernburg. 2005. A conserved checkpoint monitors meiotic chromosome synapsis in Caenorhabditis elegans. *Science.* 310:1683–1686. https://doi.org/10.1126/science.1117468

Brenner, S. 1974. The genetics of Caenorhabditis elegans. *Genetics.* 77:71–94.

Burel, J.-M., S. Besson, C. Blackburn, M. Carroll, R.K. Ferguson, H. Flynn, K. Gillen, R. Leigh, S. Li, D. Lindner, et al. 2015. Publishing and sharing multi-dimensional image data with OMERO. *Mamm. Genome.* 26:441–447. https://doi.org/10.1007/s00335-015-9587-6

Carlton, P.M., A.P. Farruggio, and A.F. Dernburg. 2006. A link between meiotic prophase progression and crossover control. *PLoS Genet.* 2:e12. https://doi.org/10.1371/journal.pgen.0020012

Carmena, M., M. Wheelock, H. Funabiki, and W.C. Earnshaw. 2012. The chromosomal passenger complex (CPC): from easy rider to the godfather of mitosis. *Nat. Rev. Mol. Cell Biol.* 13:789–803. https://doi.org/10.1038/nrm3474

Carmena, M., M.O. Lombardia, H. Ogawa, and W.C. Earnshaw. 2014. Polo kinase regulates the localization and activity of the chromosomal passenger complex in meiosis and mitosis in Drosophila melanogaster. *Open Biol.* 4:140162. https://doi.org/10.1098/rsob.140162

Chen, H., D.D. Hughes, T.A. Chan, J.W. Sedat, and D.A. Agard. 1996. IVE (Image Visualization Environment): a software platform for all three-dimensional microscopy applications. *J. Struct. Biol.* 116:56–60. https://doi.org/10.1006/jsbi.1996.0010

de Carvalho, C.E., S. Zaaijer, S. Smolikov, Y. Gu, J.M. Schumacher, and M.P. Colaiácovo. 2008. LAB-1 antagonizes the Aurora B kinase in C. elegans. *Genes Dev.* 22:2869–2885. https://doi.org/10.1101/gad.1691208

Dernburg, A.F. 2001. Here, there, and everywhere: Kinetochore function on holocentric chromosomes. *J. Cell Biol.* 153:F33–F38. https://doi.org/10.1083/jcb.153.6.F33

Dernburg, A.F., K. McDonald, G. Moulder, R. Barstead, M. Dresser, and A.M. Villeneuve. 1998. Meiotic recombination in C. elegans initiates by a conserved mechanism and is dispensable for homologous chromosome synapsis. *Cell.* 94:387–398. https://doi.org/10.1016/S0092-8674(00)81481-6

Dumont, J., K. Oegema, and A. Desai. 2010. A kinetochore-independent mechanism drives anaphase chromosome separation during acentrosomal meiosis. *Nat. Cell Biol.* 12:894–901. https://doi.org/10.1038/ncb2093

Elia, A.E.H., P. Rellos, L.F. Haire, J.W. Chao, F.J. Ivins, K. Hoepker, D. Mohammad, L.C. Cantley, S.J. Smerdon, and M.B. Yaffe. 2003. The molecular basis for phosphodependent substrate targeting and regulation of Plks by the Polo-box domain. *Cell.* 115:83–95. https://doi.org/10.1016/S0092-8674(03)00725-6

Frøkjaer-Jensen, C., M.W. Davis, C.E. Hopkins, B.J. Newman, J.M. Thummel, S.-P. Olesen, M. Grunnet, and E.M. Jorgensen. 2008. Single-copy insertion of transgenes in Caenorhabditis elegans. *Nat. Genet.* 40:1375–1383. https://doi.org/10.1038/ng.248

Fukuda, T., F. Pratto, J.C. Schimenti, J.M.A. Turner, R.D. Camerini-Otero, and C. Höög. 2012. Phosphorylation of chromosome core components may serve as axis marks for the status of chromosomal events during mammalian meiosis. *PLoS Genet.* 8:e1002485. https://doi.org/10.1371/journal.pgen.1002485

Gao, J., C. Barroso, P. Zhang, H.-M. Kim, S. Li, L. Labrador, J. Lightfoot, M.V. Gerashchenko, V.M. Labunskyy, M.-Q. Dong, et al. 2016. N-terminal acetylation promotes synaptonemal complex assembly in C. elegans. *Genes Dev.* 30:2404–2416. https://doi.org/10.1101/gad.277350.116

Ghenoiu, C., M.S. Wheelock, and H. Funabiki. 2013. Autoinhibition and Polo-dependent multisite phosphorylation restrict activity of the histone H3 kinase Haspin to mitosis. *Mol. Cell.* 52:734–745. https://doi.org/10.1016/j.molcel.2013.10.002

Harper, N.C., R. Rillo, S. Jover-Gil, Z.J. Assaf, N. Bhalla, and A.F. Dernburg. 2011. Pairing centers recruit a Polo-like kinase to orchestrate meiotic chromosome dynamics in C. elegans. *Dev. Cell.* 21:934–947. https://doi.org/10.1016/j.devcel.2011.09.001

Hayashi, M., S. Mlynarczyk-Evans, and A.M. Villeneuve. 2010. The synaptonemal complex shapes the crossover landscape through cooperative assembly, crossover promotion and crossover inhibition during Caenorhabditis elegans meiosis. *Genetics.* 186:45–58. https://doi.org/10.1534/genetics.110.115501

Herman, R.K., and C.K. Kari. 1989. Recombination between small X chromosome duplications and the X chromosome in Caenorhabditis elegans. *Genetics.* 121:723–737.

Hirsh, D., D. Oppenheim, and M. Klass. 1976. Development of the reproductive system of Caenorhabditis elegans. *Dev. Biol.* 49:200–219. https://doi.org/10.1016/0012-1606(76)90267-0

Hsu, J.Y., Z.W. Sun, X. Li, M. Reuben, K. Tatchell, D.K. Bishop, J.M. Grushcow, C.J. Brame, J.A. Caldwell, D.F. Hunt, et al. 2000. Mitotic phosphorylation of histone H3 is governed by Ipl1/aurora kinase and Glc7/PP1 phosphatase in budding yeast and nematodes. *Cell.* 102:279–291. https://doi.org/10.1016/S0092-8674(00)00034-9

Jaramillo-Lambert, A., M. Ellefson, A.M. Villeneuve, and J. Engebrecht. 2007. Differential timing of S phases, X chromosome replication, and meiotic prophase in the C. elegans germ line. *Dev. Biol.* 308:206–221. https://doi.org/10.1016/j.ydbio.2007.05.019

Jordan, P.W., J. Karppinen, and M.A. Handel. 2012. Polo-like kinase is required for synaptonemal complex disassembly and phosphorylation in mouse spermatocytes. *J. Cell Sci.* 125:5061–5072. https://doi.org/10.1242/jcs.105015

Kaitna, S., P. Pasierbek, M. Jantsch, J. Loidl, and M. Glotzer. 2002. The aurora B kinase AIR-2 regulates kinetochores during mitosis and is required for separation of homologous Chromosomes during meiosis. *Curr. Biol.* 12:798–812. https://doi.org/10.1016/S0960-9822(02)00820-5

Kawashima, S.A., Y. Yamagishi, T. Honda, K. Ishiguro, and Y. Watanabe. 2010. Phosphorylation of H2A by Bub1 prevents chromosomal instability through localizing shugoshin. *Science.* 327:172–177. https://doi.org/10.1126/science.1180189

Kelly, A.E., C. Ghenoiu, J.Z. Xue, C. Zierhut, H. Kimura, and H. Funabiki. 2010. Survivin reads phosphorylated histone H3 threonine 3 to activate the mitotic kinase Aurora B. *Science.* 330:235–239. https://doi.org/10.1126/science.1189505

Kim, Y., S.C. Rosenberg, C.L. Kugel, N. Kostow, O. Rog, V. Davydov, T.Y. Su, A.F. Dernburg, and K.D. Corbett. 2014. The chromosome axis controls meiotic events through a hierarchical assembly of HORMA domain proteins. *Dev. Cell.* 31:487–502. https://doi.org/10.1016/j.devcel.2014.09.013

Kim, Y., N. Kostow, and A.F. Dernburg. 2015. The Chromosome Axis Mediates Feedback Control of CHK-2 to Ensure Crossover Formation in C. elegans. *Dev. Cell.* 35:247–261. https://doi.org/10.1016/j.devcel.2015.09.021

Kitajima, T.S., S.A. Kawashima, and Y. Watanabe. 2004. The conserved kinetochore protein shugoshin protects centromeric cohesion during meiosis. *Nature.* 427:510–517. https://doi.org/10.1038/nature02312

Labella, S., A. Woglar, V. Jantsch, and M. Zetka. 2011. Polo kinases establish links between meiotic chromosomes and cytoskeletal forces essential for homolog pairing. *Dev. Cell.* 21:948–958. https://doi.org/10.1016/j.devcel.2011.07.011

Leung, W.-K., N. Humphryes, N. Afshar, B. Argunhan, Y. Terentyev, T. Tsubouchi, and H. Tsubouchi. 2015. The synaptonemal complex is assembled by a polySUMOylation-driven feedback mechanism in yeast. *J. Cell Biol.* 211:785–793. https://doi.org/10.1083/jcb.201506103

Libuda, D.E., S. Uzawa, B.J. Meyer, and A.M. Villeneuve. 2013. Meiotic chromosome structures constrain and respond to designation of crossover sites. *Nature.* 502:703–706. https://doi.org/10.1038/nature12577

Lui, D.Y., and M.P. Colaiácovo. 2013. Meiotic development in Caenorhabditis elegans. *Adv. Exp. Med. Biol.* 757:133–170. https://doi.org/10.1007/978-1-4614-4015-4_6

MacQueen, A.J., M.P. Colaiácovo, K. McDonald, and A.M. Villeneuve. 2002. Synapsis-dependent and -independent mechanisms stabilize homolog pairing during meiotic prophase in C. elegans. *Genes Dev.* 16:2428–2442. https://doi.org/10.1101/gad.1011602

MacQueen, A.J., C.M. Phillips, N. Bhalla, P. Weiser, A.M. Villeneuve, and A.F. Dernburg. 2005. Chromosome sites play dual roles to establish homologous synapsis during meiosis in C. elegans. *Cell.* 123:1037–1050. https://doi.org/10.1016/j.cell.2005.09.034

Martinez-Perez, E., M. Schvarzstein, C. Barroso, J. Lightfoot, A.F. Dernburg, and A.M. Villeneuve. 2008. Crossovers trigger a remodeling of meiotic chromosome axis composition that is linked to two-step loss of sister chromatid cohesion. *Genes Dev.* 22:2886–2901. https://doi.org/10.1101/gad.1694108

McKim, K.S., K. Peters, and A.M. Rose. 1993. Two types of sites required for meiotic chromosome pairing in Caenorhabditis elegans. *Genetics.* 134:749–768.

Melters, D.P., L.V. Paliulis, I.F. Korf, and S.W.L. Chan. 2012. Holocentric chromosomes: convergent evolution, meiotic adaptations, and genomic analysis. *Chromosome Res.* 20:579–593. https://doi.org/10.1007/s10577-012-9292-1

Nabeshima, K., A.M. Villeneuve, and M.P. Colaiácovo. 2005. Crossing over is coupled to late meiotic prophase bivalent differentiation through asymmetric disassembly of the SC. *J. Cell Biol.* 168:683–689. https://doi.org/10.1083/jcb.200410144

Nadarajan, S., T.J. Lambert, E. Altendorfer, J. Gao, M.D. Blower, J.C. Waters, and M.P. Colaiácovo. 2017. Polo-like kinase-dependent phosphorylation of the synaptonemal complex protein SYP-4 regulates double-strand break formation through a negative feedback loop. *eLife.* 6:e23437. https://doi.org/10.7554/eLife.23437

Oegema, K., A. Desai, S. Rybina, M. Kirkham, and A.A. Hyman. 2001. Functional analysis of kinetochore assembly in *Caenorhabditis elegans*. *J. Cell Biol.* 153:1209–1226. https://doi.org/10.1083/jcb.153.6.1209

Pasierbek, P., M. Jantsch, M. Melcher, A. Schleiffer, D. Schweizer, and J. Loidl. 2001. A Caenorhabditis elegans cohesion protein with functions in meiotic chromosome pairing and disjunction. *Genes Dev.* 15:1349–1360. https://doi.org/10.1101/gad.192701

Pattabiraman, D., B. Roelens, A. Woglar, and A.M. Villeneuve. 2017. Meiotic recombination modulates the structure and dynamics of the synaptonemal complex during C. elegans meiosis. *PLoS Genet.* 13:e1006670. https://doi.org/10.1371/journal.pgen.1006670

Penkner, A.M., A. Fridkin, J. Gloggnitzer, A. Baudrimont, T. Machacek, A. Woglar, E. Csaszar, P. Pasierbek, G. Ammerer, Y. Gruenbaum, and V. Jantsch. 2009. Meiotic chromosome homology search involves modifications of the nuclear envelope protein Matefin/SUN-1. *Cell.* 139:920–933. https://doi.org/10.1016/j.cell.2009.10.045

Phillips, C.M., and A.F. Dernburg. 2006. A family of zinc-finger proteins is required for chromosome-specific pairing and synapsis during meiosis in C. elegans. *Dev. Cell.* 11:817–829. https://doi.org/10.1016/j.devcel.2006.09.020

Phillips, C.M., C. Wong, N. Bhalla, P.M. Carlton, P. Weiser, P.M. Meneely, and A.F. Dernburg. 2005. HIM-8 binds to the X chromosome pairing center and mediates chromosome-specific meiotic synapsis. *Cell.* 123:1051–1063. https://doi.org/10.1016/j.cell.2005.09.035

Phillips, C.M., K.L. McDonald, and A.F. Dernburg. 2009. Cytological analysis of meiosis in Caenorhabditis elegans. *Methods Mol. Biol.* 558:171–195. https://doi.org/10.1007/978-1-60761-103-5_11

Qian, J., B. Lesage, M. Beullens, A. Van Eynde, and M. Bollen. 2011. PP1/Repo-man dephosphorylates mitotic histone H3 at T3 and regulates chromosomal aurora B targeting. *Curr. Biol.* 21:766–773. https://doi.org/10.1016/j.cub.2011.03.047

Rockman, M.V., and L. Kruglyak. 2009. Recombinational landscape and population genomics of Caenorhabditis elegans. *PLoS Genet.* 5:e1000419. https://doi.org/10.1371/journal.pgen.1000419

Rogers, E., J.D. Bishop, J.A. Waddle, J.M. Schumacher, and R. Lin. 2002. The aurora kinase AIR-2 functions in the release of chromosome cohesion in *Caenorhabditis elegans* meiosis. *J. Cell Biol.* 157:219–229. https://doi.org/10.1083/jcb.200110045

Rosu, S., K.A. Zawadzki, E.L. Stamper, D.E. Libuda, A.L. Reese, A.F. Dernburg, and A.M. Villeneuve. 2013. The C. elegans DSB-2 protein reveals a regulatory network that controls competence for meiotic DSB formation and promotes crossover assurance. *PLoS Genet.* 9:e1003674. https://doi.org/10.1371/journal.pgen.1003674

Saito, T.T., F. Mohideen, K. Meyer, J.W. Harper, and M.P. Colaiácovo. 2012. SLX-1 is required for maintaining genomic integrity and promoting meiotic noncrossovers in the Caenorhabditis elegans germline. *PLoS Genet.* 8:e1002888. https://doi.org/10.1371/journal.pgen.1002888

Saito, T.T., D.Y. Lui, H.-M. Kim, K. Meyer, and M.P. Colaiácovo. 2013. Interplay between structure-specific endonucleases for crossover control during Caenorhabditis elegans meiosis. *PLoS Genet.* 9:e1003586. https://doi.org/10.1371/journal.pgen.1003586

Sato-Carlton, A., X. Li, O. Crawley, S. Testori, E. Martinez-Perez, A. Sugimoto, and P.M. Carlton. 2014. Protein phosphatase 4 promotes chromosome pairing and synapsis, and contributes to maintaining crossover competence with increasing age. *PLoS Genet.* 10:e1004638. https://doi.org/10.1371/journal.pgen.1004638

Schild-Prüfert, K., T.T. Saito, S. Smolikov, Y. Gu, M. Hincapie, D.E. Hill, M. Vidal, K. McDonald, and M.P. Colaiácovo. 2011. Organization of the synaptonemal complex during meiosis in Caenorhabditis elegans. *Genetics.* 189:411–421. https://doi.org/10.1534/genetics.111.132431

Schindelin, J., I. Arganda-Carreras, E. Frise, V. Kaynig, M. Longair, T. Pietzsch, S. Preibisch, C. Rueden, S. Saalfeld, B. Schmid, et al. 2012. Fiji: an open-source platform for biological-image analysis. *Nat. Methods.* 9:676–682. https://doi.org/10.1038/nmeth.2019

Severson, A.F., and B.J. Meyer. 2014. Divergent kleisin subunits of cohesin specify mechanisms to tether and release meiotic chromosomes. *eLife.* 3:e03467. https://doi.org/10.7554/eLife.03467

Stamper, E.L., S.E. Rodenbusch, S. Rosu, J. Ahringer, A.M. Villeneuve, and A.F. Dernburg. 2013. Identification of DSB-1, a protein required for initiation of meiotic recombination in Caenorhabditis elegans, illuminates a crossover assurance checkpoint. *PLoS Genet.* 9:e1003679. https://doi.org/10.1371/journal.pgen.1003679

Tzur, Y.B., C. Egydio de Carvalho, S. Nadarajan, I. Van Bostelen, Y. Gu, D.S. Chu, I.M. Cheeseman, and M.P. Colaiácovo. 2012. LAB-1 targets PP1 and restricts Aurora B kinase upon entrance into meiosis to promote sister chromatid cohesion. *PLoS Biol.* 10:e1001378. https://doi.org/10.1371/journal.pbio.1001378

Villeneuve, A.M. 1994. A cis-acting locus that promotes crossing over between X chromosomes in Caenorhabditis elegans. *Genetics.* 136:887–902.

Wang, F., J. Dai, J.R. Daum, E. Niedzialkowska, B. Banerjee, P.T. Stukenberg, G.J. Gorbsky, and J.M.G. Higgins. 2010. Histone H3 Thr-3 phosphorylation by Haspin positions Aurora B at centromeres in mitosis. *Science.* 330:231–235. https://doi.org/10.1126/science.1189435

Wang, F., N.P. Ulyanova, M.S. van der Waal, D. Patnaik, S.M.A. Lens, and J.M.G. Higgins. 2011. A positive feedback loop involving Haspin and Aurora B promotes CPC accumulation at centromeres in mitosis. *Curr. Biol.* 21:1061–1069. https://doi.org/10.1016/j.cub.2011.05.016

Woglar, A., A. Daryabeigi, A. Adamo, C. Habacher, T. Machacek, A. La Volpe, and V. Jantsch. 2013. Matefin/SUN-1 phosphorylation is part of a surveillance mechanism to coordinate chromosome synapsis and recombination with meiotic progression and chromosome movement. *PLoS Genet.* 9:e1003335. https://doi.org/10.1371/journal.pgen.1003335

Yamagishi, Y., T. Honda, Y. Tanno, and Y. Watanabe. 2010. Two histone marks establish the inner centromere and chromosome bi-orientation. *Science.* 330:239–243. https://doi.org/10.1126/science.1194498

Yokoo, R., K.A. Zawadzki, K. Nabeshima, M. Drake, S. Arur, and A.M. Villeneuve. 2012. COSA-1 reveals robust homeostasis and separable licensing and reinforcement steps governing meiotic crossovers. *Cell.* 149:75–87. https://doi.org/10.1016/j.cell.2012.01.052

Zalevsky, J., A.J. MacQueen, J.B. Duffy, K.J. Kemphues, and A.M. Villeneuve. 1999. Crossing over during Caenorhabditis elegans meiosis requires a conserved MutS-based pathway that is partially dispensable in budding yeast. *Genetics.* 153:1271–1283.

Zickler, D., and N. Kleckner. 1999. Meiotic chromosomes: integrating structure and function. *Annu. Rev. Genet.* 33:603–754. https://doi.org/10.1146/annurev.genet.33.1.603

Sato-Carlton et al., https://doi.org/10.1083/jcb.201707161

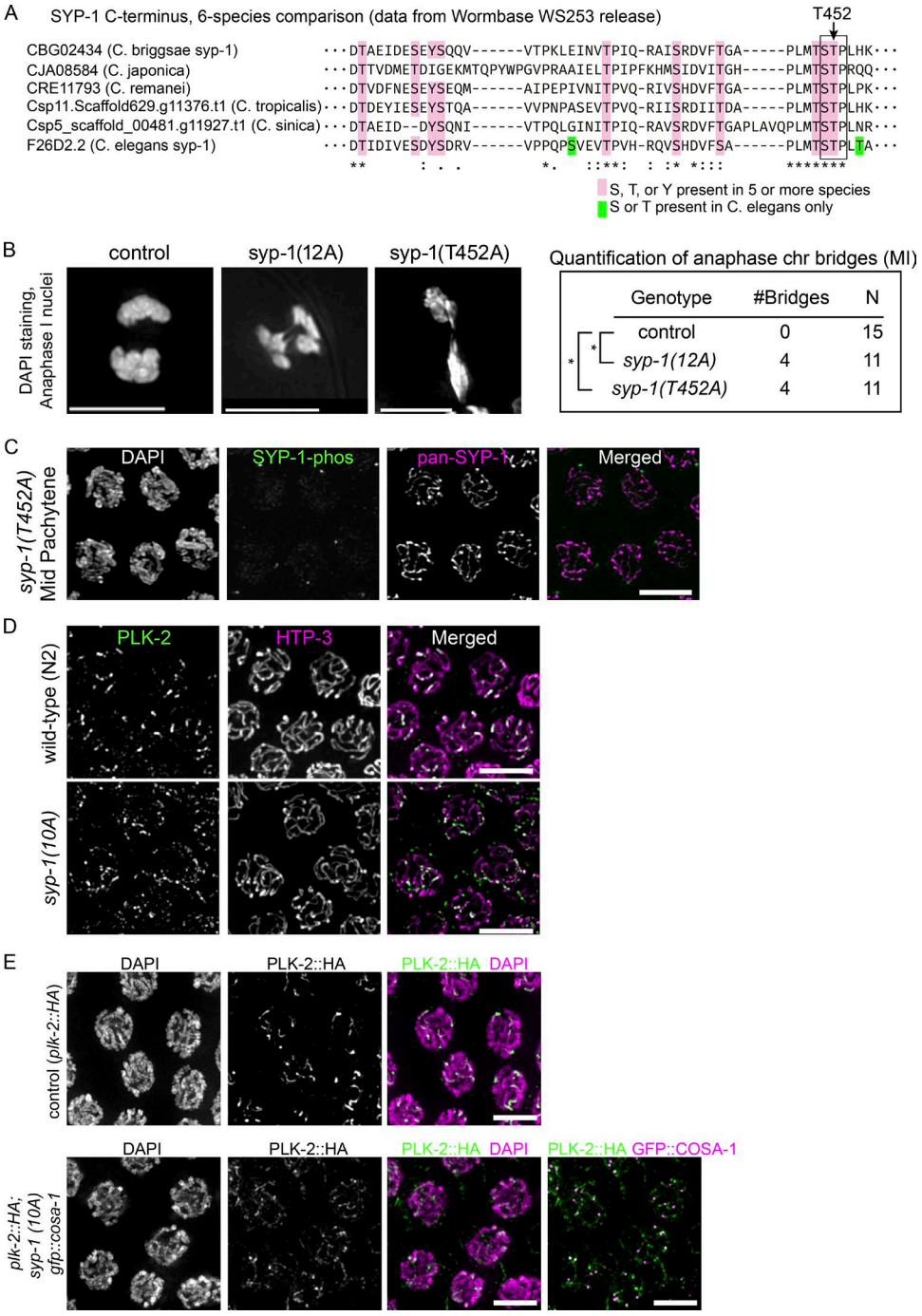

Figure S1. **Conservation of the SYP-1 PBD-binding motif among six nematode species, and characterization of *syp-1* phospho mutants. (A)** C-terminal amino acid sequence of SYP-1 and its orthologues in six nematode species. Pink highlights Ser, Thr, or Tyr residues conserved in five or more species; green highlights Ser or Thr only present in *C. elegans*. The conserved PBD-binding motif STP is boxed. **(B)** DAPI staining images of anaphase I oocyte nuclei in *syp-1(wt); syp-1(me17)*, *syp-1(12A); syp-1(me17)*, and *syp-1(T452A); syp-1(me17)* mutants. Table shows the number of anaphases with visible bridges and the total number of anaphases scored (N). *, P = 0.02207, Fisher's exact test. Bars, 5 µm. **(C)** Loss of SYP-1-phos staining in *syp-1(T452A)* mutants. SYP-1-phos is shown in green, and pan-SYP-1 is shown in magenta. Bar, 5 µm. **(D)** PLK-2 immunostaining in late pachytene nuclei in wild-type (top) and *syp-1(10A); syp-1(me17)* (bottom) gonads. Bars, 5 µm. **(E)** Late pachytene nuclei in control (*plk-2::HA*) and *plk-2::HA; syp-1(10A) gfp::cosa-1; syp-1(me17)* gonads were fixed and stained with antibodies against HA (green) or HA (green) and GFP (magenta) for the 10A mutant. PLK-2::HA is detected at reduced levels on the SC in 10A mutants. Bars, 5 µm.

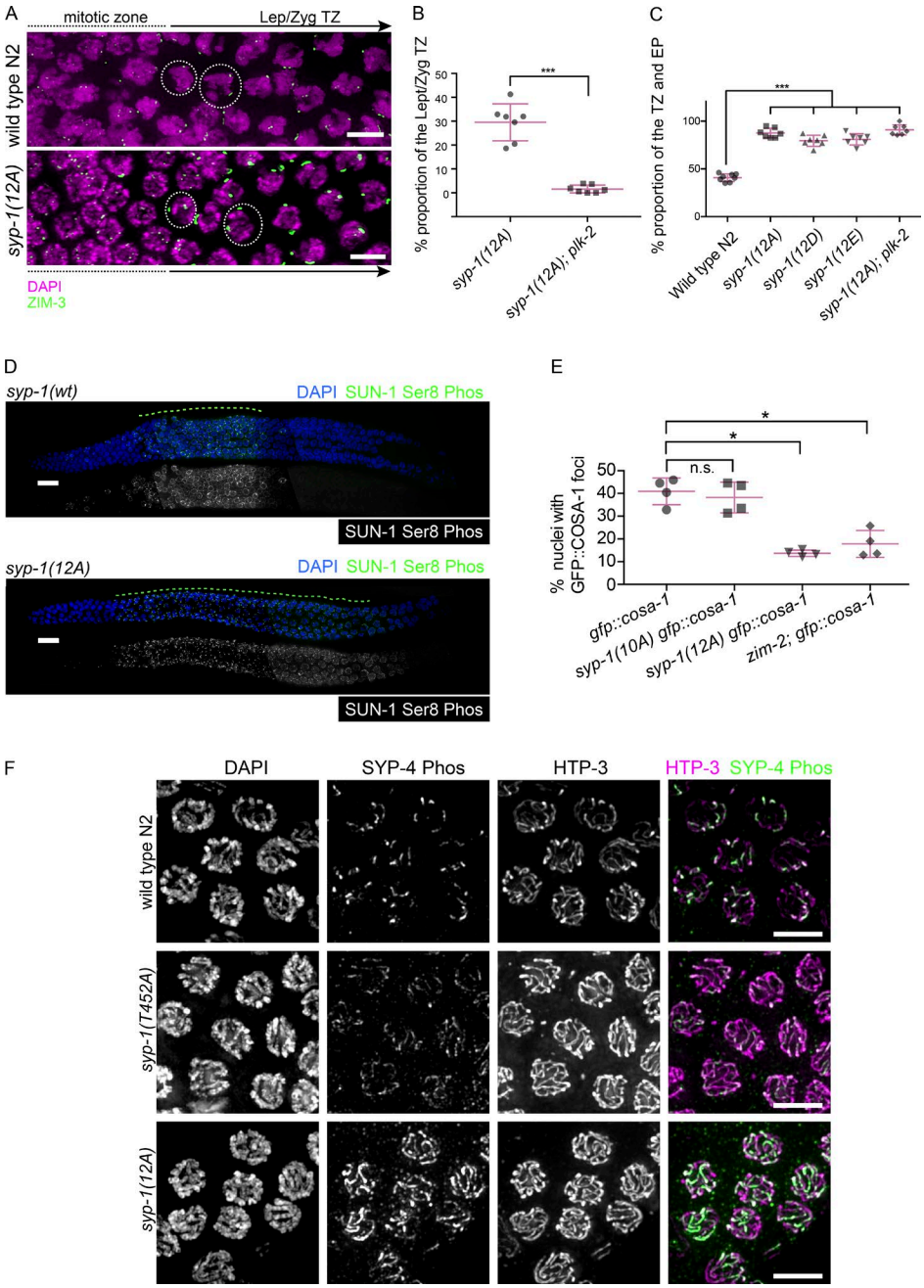

Figure S2. **Characterization of *syp-1* phospho mutants. (A)** Homologous chromosome pairing is normal in *syp-1* nonphosphorylatable mutants. Pairing was visualized by immunostaining of ZIM-3 (green), which binds to the PCs of chromosomes I and IV in the wild type and *syp-1(12A); syp-1(me17)* mutant. As meiocytes progress from the zone containing mitotically proliferating cells (left) to meiotic prophase (right), unpaired homologous chromosomes (four ZIM-3 foci per nucleus) become paired (two foci per nucleus) in the leptotene/zygotene TZ. DNA is counterstained with DAPI (magenta). Bars, 5 µm. **(B)** PLK-2 is required to extend the TZ in *syp-1(12A)* mutants. PLK-2 is essential to induce chromosome clustering, a defining feature of TZ nuclei, and very few or almost no TZ nuclei are found in *plk-2* mutants (Harper et al., 2011; Labella et al., 2011). The proportion of the TZ was calculated by dividing the length of the TZ by the length of TZ + pachytene. The *plk-2(ok1936); syp-1(12A)* double-mutant gonads similarly possessed few or no leptotene/zygotene nuclei compared with *syp-1(12A)* controls. ***, $P < 0.001$, Mann–Whitney test. Error bars indicate mean and SD. **(C)** The proportion of combined TZ and early pachytene region, marked by SUN-1 Ser8 phosphorylation, was extended in *syp-1(12D); syp-1(me17)*, *syp-1(12E); syp-1(me17)*, and *plk-2(ok1936); syp-1(12A)* double mutants to a similar level as *syp-1(12A); syp-1(me17)* mutants as well as *plk-2* mutant gonads, previously reported to have an extended region of SUN-1 Ser8 phosphorylation (Harper et al., 2011). ***, $P < 0.0001$, Mann–Whitney test. Error bars indicate mean and SD. **(D)** Representative gonad images of *syp-1 (wt); syp-1(me17)* and *syp-1(12A); syp-1(me17)* animals with DAPI (blue) and SUN-1 Ser8-phos staining (green in the top panel and white in the lower panel). The gonad region with SUN-1 Ser8-phos staining is highlighted with a dotted line. Bars, 15 µm. **(E)** The appearance of GFP::COSA-1 foci is delayed in *syp-1(12A)* but not in *syp-1(10A)* mutants. Quantification of the proportion of nuclei with GFP::COSA-1 in *gfp::cosa-1, gfp::cosa-1 syp-1(10A); syp-1(me17), gfp::cosa-1 syp-1(12A); syp-1(me17)* and *gfp::cosa-1; zim-2 (tm574)*. The proportion was calculated by dividing the length of the gonad region positive for GFP::COSA-1 by the combined length of the TZ and pachytene. The *zim-2* mutant is defective for homologous pairing of chromosome V, and delays entrance into late pachytene by activating a meiotic checkpoint (Phillips and Dernburg, 2006). This allows *zim-2* to be used as a positive control for delayed GFP::COSA-1 formation. For each genotype, four gonads were scored. Error bars show SD. *, $P < 0.05$, Mann–Whitney test. Error bars indicate mean and SD. **(F)** SYP-4-phos immunostaining of late pachytene nuclei in wild type N2, *syp-1(T452A); syp-1(me17)*, and *syp-1(12A); syp-1(me17)* mutants. Bars, 5 µm.

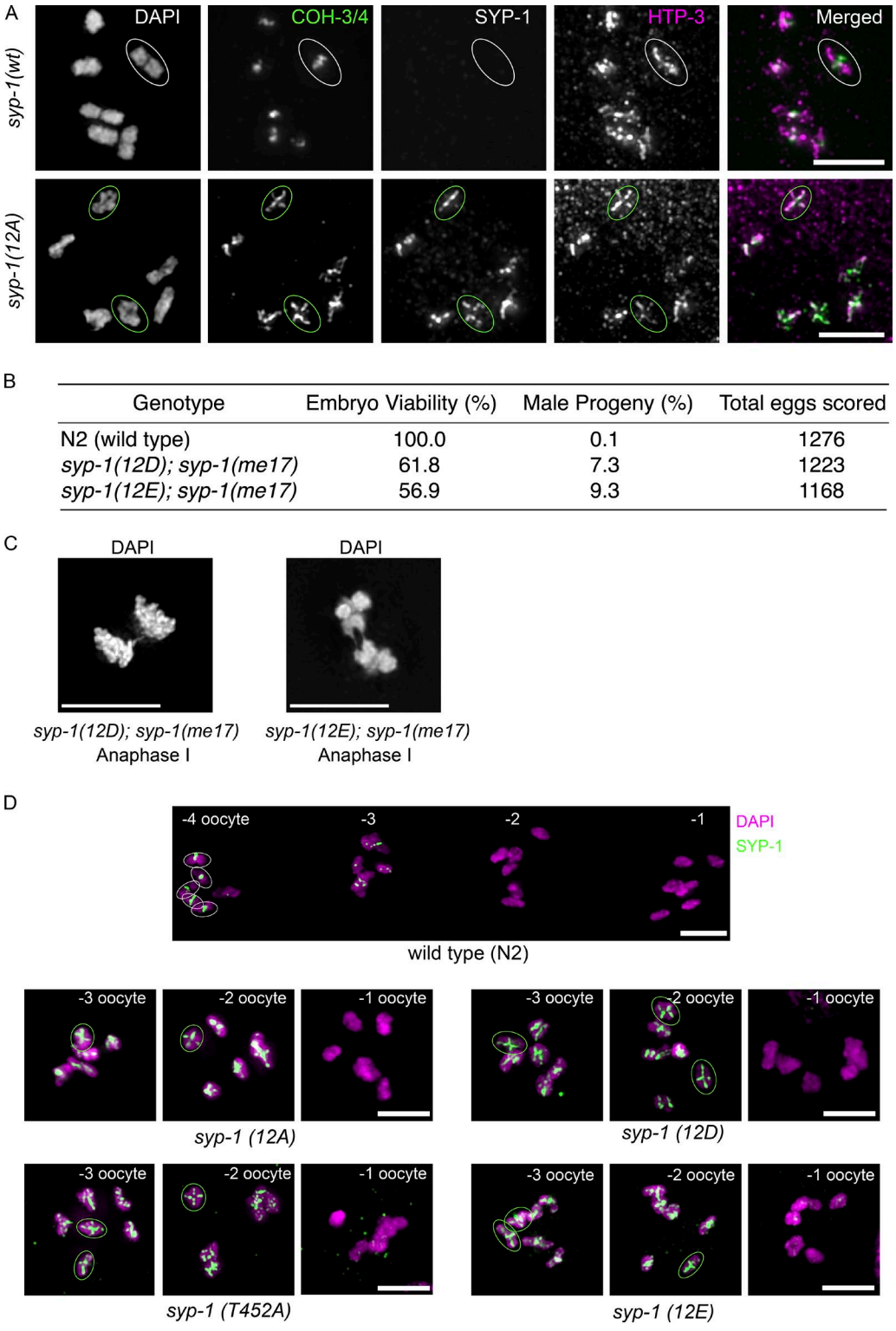

Genotype	Embryo Viability (%)	Male Progeny (%)	Total eggs scored
N2 (wild type)	100.0	0.1	1276
syp-1(12D); syp-1(me17)	61.8	7.3	1223
syp-1(12E); syp-1(me17)	56.9	9.3	1168

Figure S3. **Aberrant persistence of SYP-1 and cohesin subunits COH-3/4 in diakinesis nuclei in *syp-1(12A)* mutants. (A)** Immunostaining of −1 oocyte nuclei with COH-3/4 (green), SYP-1 (grayscale), and HTP-3 (magenta) antibodies. COH-3/4 aberrantly persists on both long and short arms in −1 oocyte nuclei in *syp-1(12A); syp-1(me17)* mutants. **(B)** Percentage of viability and male progeny of worms with the indicated genotypes. For each mutant, all 12 Ser/Thr/Tyr phosphosites are converted to either Asp or Glu. **(C)** Oocyte anaphase I nucleus with anaphase chromosome bridges in *syp-1(12D); syp-1(me17)* or *syp-1(12E); syp-1(me17)* mutants. Bars, 5 µm. **(D)** Pan-SYP-1 staining (green) of diakinesis nuclei in wild-type, *syp-1(12A); syp-1(me17)*, *syp-1(T452A); syp-1(me17)*, *syp-1(12D); syp-1(me17)*, and *syp-1(12E); syp-1(me17)* animals. SYP-1 is normally detected on short arms until the −4 or −3 oocyte stage and disappears by the −2 oocyte stage in the wild-type, whereas it always persists on both arms until the −2 or −1 oocyte stage in the *syp-1* phosphomutants indicated. DNA is counterstained with DAPI (magenta). Bars, 5 µm.

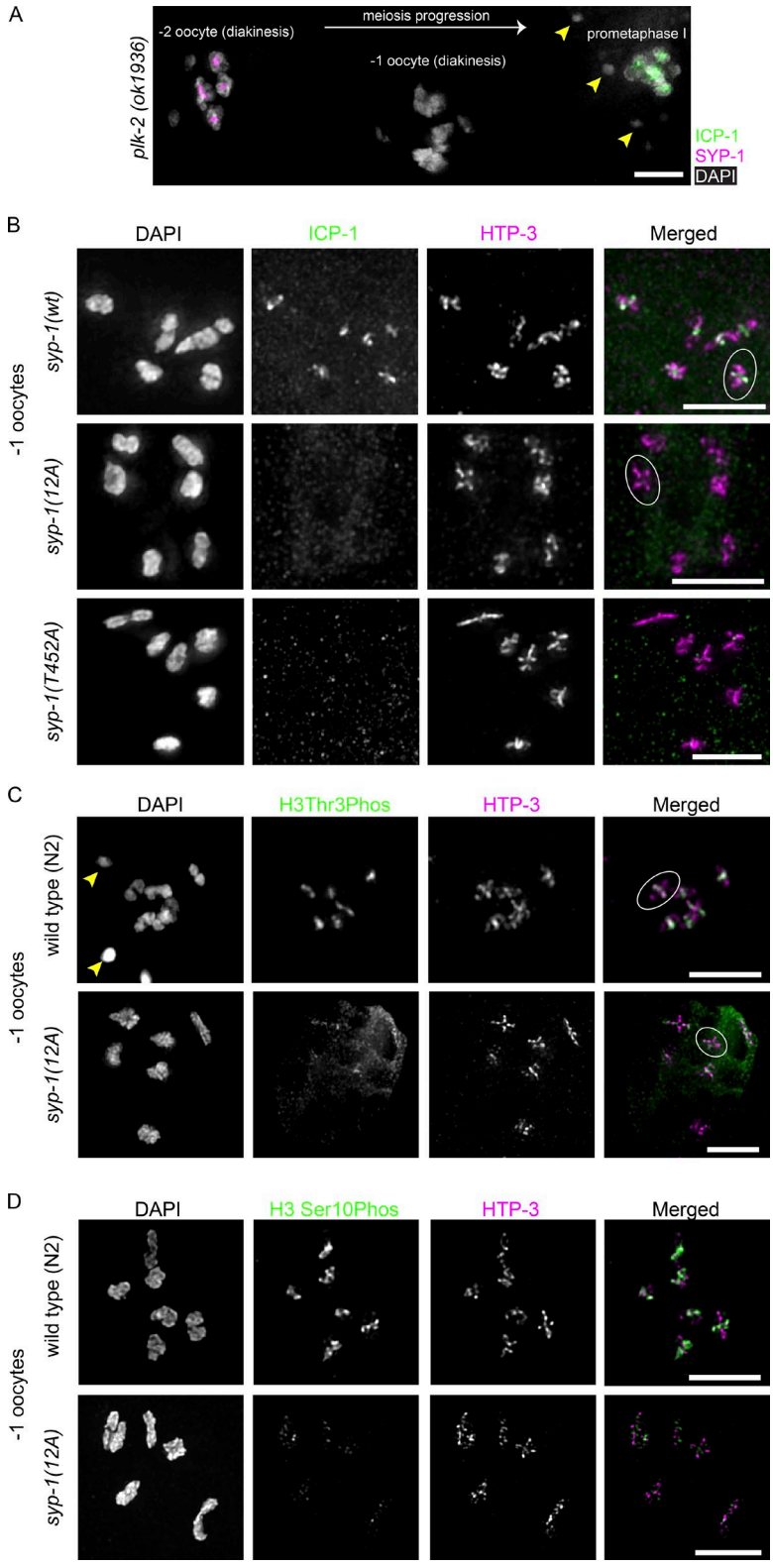

Figure S4. **Mislocalization of CPC components and CPC-related histone marks in *syp-1(12A)* mutants. (A)** Immunostaining of -2, -1, and prometaphase oocyte nuclei with SYP-1 (magenta) and ICP-1 (green) antibodies in the *plk-2 (ok1936)* gonad. Although ICP-1 is not detected in −1 oocyte nuclei, accumulation of ICP-1 is found in oocyte prometaphase nuclei. Arrowheads indicate sperm nuclei. **(B and C)** Maximum-intensity projection images of the whole −1 oocyte nucleus with ICP-1 (green, top) or H3T3ph (green, middle) and HTP-3 (magenta) staining in *syp-1(wt)* (top), *syp-1(me17); syp-1(12A)* (middle), and *syp-1(me17)* (B and C, bottom) and *syp-1(T452A); syp-1(me17)* (B) animals. Partial projections of the chromosomes indicated by circles are presented with the long axis rotated to the vertical in Fig. 4 (B and C). Both ICP-1 and H3T3ph staining levels are reduced in 12A mutants. Arrowheads indicate sperm DNA. **(D)** Immunostaining of histone H3S10ph (green) and HTP-3 (magenta) in −1 oocyte nuclei of wild-type N2 and *syp-1(12A); syp-1(me17)* animals. H3S10ph staining levels are reduced in 12A mutants. Bars, 5 µm.

Provided online is Table S1, in Excel, showing the details and counts of phosphopeptides obtained from mass spectrometry. For all phosphopeptides detected only once, mass spectrometry spectra were manually examined, and peptides with high-confidence assignment are indicated. The tandem mass spectrometry spectra showing m/z and intensity values for these manually reviewed peptides are shown with accompanying spectrum images in sheets 2–8 in the same Excel file.